Geophysical Journal International

Geophys. J. Int. (2014) **199,** 1633–1654 doi: 10.1093/gji/ggu355
GJI Seismology

Flat versus normal subduction zones: a comparison based on 3-D regional traveltime tomography and petrological modelling of central Chile and western Argentina (29°–35°S)

M. Marot,[1] T. Monfret,[1] M. Gerbault,[1] G. Nolet,[1] G. Ranalli[2] and M. Pardo[3]

[1] *Géoazur, UNSA, IRD, CNRS, OCA (UMR* 7329*),* 250 *Albert Einstein, F-*06560 *Valbonne, France. E-mail: marianne_marot@hotmail.com*
[2] *Department of Earth Sciences, Carleton University,* 1125 *Colonel By Drive, Ottawa, ON* K1S 5B*, Canada*
[3] *Departamento de Geofísica, Universidad de Chile, Blanco Encalada* 2002*, Santiago, Chile*

Accepted 2014 September 8. Received 2014 September 3; in original form 2014 March 24

SUMMARY

Our study compares the seismic properties between the flat and normal subduction regions in central Chile, to better understand the links between the slab geometry, surface deformation and the deeper structures. In comparison with previous studies, we show the most complete 3-D regional seismic tomography images for this region, in which we use (1) a larger seismic data set compiled from several short-term seismic catalogues, (2) a denser seismic array allowing a better resolution of the subduction zone from the trench to the backarc and into the upper ∼30 km of the slab and (3) a starting 1-D background velocity model specifically calculated for this region and refined over the years. We assess and discuss our tomography results using regional seismic attenuation models and estimating rock types on the basis of pressure and temperature conditions computed from thermomechanical models. Our results show significant seismic differences between the flat and normal subduction zones. As expected, the faster seismic velocities and increased seismicity within the flat slab and overriding lithosphere are generally consistent with a cooler thermal state. Our results are also consistent with dehydration of the mantle above the subducted Juan Fernandez Ridge at the eastern tip of the flat slab segment, indicating that the latter retains some fluids during subduction. However, fluids in the upper portion of the flat slab segment are not seismically detected, since we report instead fast slab seismic velocities which contradict the argument of its buoyancy being the cause of horizontal subduction. The forearc region, above the flat slab, exhibits high *Vs* and very low *Vp*/*Vs* ratios, uncorrelated with typical rock compositions, increased density or reduced temperature; this feature is possibly linked with the aftershock effects of the *M*w7.1 1997 Punitaqui earthquake, the flat slab geometry and/or seismic anisotropy. At the surface, the seismic variations correlate with the geological terranes. The Andean crust is strongly reduced in seismic velocities along the La Ramada–Aconcagua deformation belt, suggesting structural damage. Slow seismic velocities along the Andean Moho match non-eclogitized hydrated rocks, consistent with a previous delamination event or a felsic composition, which in turn supports the extent of the Chilenia terrane at these depths. We confirm previous studies that suggest that the Cuyania terrane in the backarc region is mafic and contains an eclogitized lower crust below 50-km depth. We also hypothesize major Andean basement detachment faults (or shear zones) to extend towards the plate interface and canalize slab-derived fluids into the continental crust.

Key words: Seismicity and tectonics; Seismic tomography; Subduction zone processes; Dynamics: seismotectonics; South America.

1 INTRODUCTION

Along the South American margin, spatial correlations exist between subducting oceanic features (ridges, plateaus, fracture zones), volcanic arc gaps, backarc basement uplifts and past or present occurrences of flat subduction (Skinner & Clayton 2013). The two most typical present-day flat slabs are beneath Peru and central Chile, both attached to the Nazca Plate along the South American margin. Nevertheless, the cause for their formation is still debated.

The central Chilean 'Pampean' flat slab (∼29°–32.5°S) is perhaps the best documented so far, since the region has the advantage of a high microseismic activity, good geological exposure levels,

advanced structural evolution and has been affected by shallowly dipping subduction for a relatively long time (15–18 Ma; Kay & Mpodozis 2002; Ramos *et al.* 2002). It is associated with the subduction of relatively young (35–40 Ma) and hydrated lithosphere (Kopp *et al.* 2004) and of the Juan Fernandez hotspot seamount Ridge (JFR) beneath the thick continental South American lithosphere. Both the region's high seismicity and the slab's rapid geometrical transition (from plunging 30° to 0°) render this location ideal to study the seismic properties and anomalies associated to flat subduction.

In normal subduction circumstances, conventional slab dehydration processes take place due to high temperature distribution at depth, resulting in arc volcanism, seismicity and weakening of the continental crust. However, in the case of flat subduction, the asthenosphere is expelled during slab flattening, significantly cooling the system, particularly the upper lithosphere (Kay & Mpodozis 2002; Ramos *et al.* 2002; Grevemeyer *et al.* 2003). In the case of the central Chilean flat slab, the flattening is associated with changes in (i) plate coupling forces, (ii) compressional stresses farther inland, (iii) topography, (iv) seismicity in the backarc, forearc, plate interface and slab (including a Double Seismic Zone, Marot *et al.* 2013) and (v) cessation of arc volcanism (Kay & Abbruzzi 1996; Kay & Mpodozis 2002; Ramos *et al.* 2002; Martinod *et al.* 2013).

While the slab's buoyancy and thermomechanical properties are commonly considered the dominant parameters influencing changes in slab geometry, there is a growing consensus that the rheology of the upper plate also plays a non-negligible role in the occurrence of flat subductions (e.g. Van Hunen *et al.* 2001, 2002, 2004; Espurt *et al.* 2008; Gerbault *et al.* 2009; Manea *et al.* 2012).

Whereas the processes and timing of slab flattening are well constrained from available data on backarc basement uplift and eastward volcanic arc migration (Ramos *et al.* 2002; Alvarado *et al.* 2007), the factors that triggered flat subduction and maintained it for at least 6 Myr (Kay *et al.* 1991; Kay & Abbruzzi 1996), as well as its relationship with the deep composition and deformation of the overriding lithosphere, are ill-constrained and multiple paradoxes exist. Although there appears to be an obvious influence of the JFR, it is deemed too small in size to have caused by itself the total extent of the flat slab (200–250 km in length) (e.g. Yáñez *et al.* 2002; Martinod *et al.* 2010).

In this context, our study images the deep seismic structure of the continental lithosphere in order to better understand its interactions with the flat slab, and the possible mechanisms causing and maintaining it. To this end, we performed 3-D regional seismic tomography of *P*- and *S*-wave residual traveltimes using local earthquakes recorded by four temporary seismic campaigns (OVA99, CHARGE, CHARSME, CHASE) to compare the normal (27°–30°) subduction region south of 33.5°S (taken to represent conventional subduction conditions) with the flat subduction zone, between 31° and 32°S. We then compared our absolute seismic velocities with those predicted for subduction-type rocks, using the Hacker & Abers (2004) worksheet, at appropriate pressure and temperature (*P*–*T*) conditions obtained from thermomechanical modelling. We also compare our results with those of Wagner *et al.* (2005, 2006), who performed a similar experiment for this region using only the CHARGE database. As an improvement to their work, our study incorporates a much larger earthquake catalogue (3770 events) representing different time periods and resulting in greater ray coverage, increased resolution and a longer temporal view of the seismic properties of the lithosphere. Furthermore, our results include the continental crust and the upper portion of the slab lithosphere, which could not be interpreted in their models due to lack of data and poor resolution. We also used seismic attenuation models for the region, calculated by Deshayes (2008) from the OVA99 and CHARSME catalogues, to strengthen our interpretations of the nature of our observed velocity perturbations. Our work offers a finer scale, broader and more complete image of the region's subduction system.

We confirm previous interpretations of a generally cold, dry and Mg-rich continental mantle, and an eclogitized Cuyania lower crust in the backarc. However, we also suggest localized continental mantle hydration above the subducting JFR which reflects dehydration processes, and also the absence of an eclogitized Andean lower crust. The flat slab segment exhibits fast seismic properties only explained with dense eclogite or peridotite, both denser than normal mantle rocks, contradicting the argument of buoyancy-driven horizontal subduction. We also note correlations between geological terrane boundaries and seismic velocity variations, high-*Vp*/*Vs* regions and major basement shear zones and, correlations between very low *Vp*/*Vs* forearc anomalies and the Punitaqui aftershock region within the flat slab area.

2 TECTONIC AND GEOLOGICAL SETTINGS

The Nazca Plate subducts beneath central Chile and western Argentina (29°–35°S) at a current convergence rate of 6.7 ± 0.2 cm a^{-1} in the N78°E direction (Fig. 1; Kendrick *et al.* 2003). The region between 30°S and the subducting JFR path (∼32.5°S) is defined as the flat slab region (Fig. 1c). The flat slab segment underplates the continental lithosphere at 100–120-km depth for 200–300 km eastwards, before resubducting at 68°W with a 30°-dip angle (Fig. 1d; Barazangi & Isacks 1976; Cahill & Isacks 1992; Pardo *et al.* 2002; Anderson *et al.* 2007). The flat slab segment is bounded to the north by a gentle along-strike transition towards a normal 30°-dip angle, whereas to the south, the transition is more abrupt (only ∼100-km wide, 32.5°–33.5°S, Fig. 1a; Cahill & Isacks 1992; Araujo & Suarez 1994; Giambiagi & Ramos 2002; Pardo *et al.* 2002) and is more often interpreted as a sharp bend rather than a tear (Araujo & Suarez 1994; Wagner *et al.* 2005; Pesicek *et al.* 2012).

At ∼25 Ma, the Farallon Plate broke-up into the smaller Cocos and Nazca plates. At ∼18–15 Ma, the Nazca Plate in central Chile began shallowing from ∼45° to 30°-dip angle (Ramos *et al.* 2002). Around 12–10 Ma, the southward migrating JFR intercepted the central Chilean trench, slab shallowing increased and the main arc volcanism ceased completely at 9 Ma (Kay & Mpodozis 2002). The JFR currently subducts along the trench at 32.5°–33°S (Fig. 1a) since 11 Ma (Yáñez *et al.* 2002), and the present flat slab geometry (Fig. 1c) is believed to have been achieved since 6 Ma (Kay *et al.* 1991; Kay & Abbruzzi 1996).

Since the onset of slab shallowing below South America, eastward volcanic arc migration and increasing compressional stresses have been invoked to explain strong tectonic uplift and intense shortening (up to ∼130–150 km, compared to <100 km further south, Allmendinger *et al.* 1997; Kley & Monaldi 1998; Alvarado *et al.* 2007; Martinod *et al.* 2013). The South American overriding plate is described by five different morpho-tectono-structural-geological provinces (west to east) (Fig. 1b): the Coastal Cordillera (forearc), the Principal and Frontal Cordilleras (present-day Andes), the Precordillera (foothill) and the Sierra Pampeanas (backarc).

Significant changes occur between the flat and normal subduction zones, in association with the shift in slab geometry. To mention only a few, in comparison with the flat slab region (Fig. 1): (i) the trench's strike rotates from N20°E to N5°E, (ii) the temperature

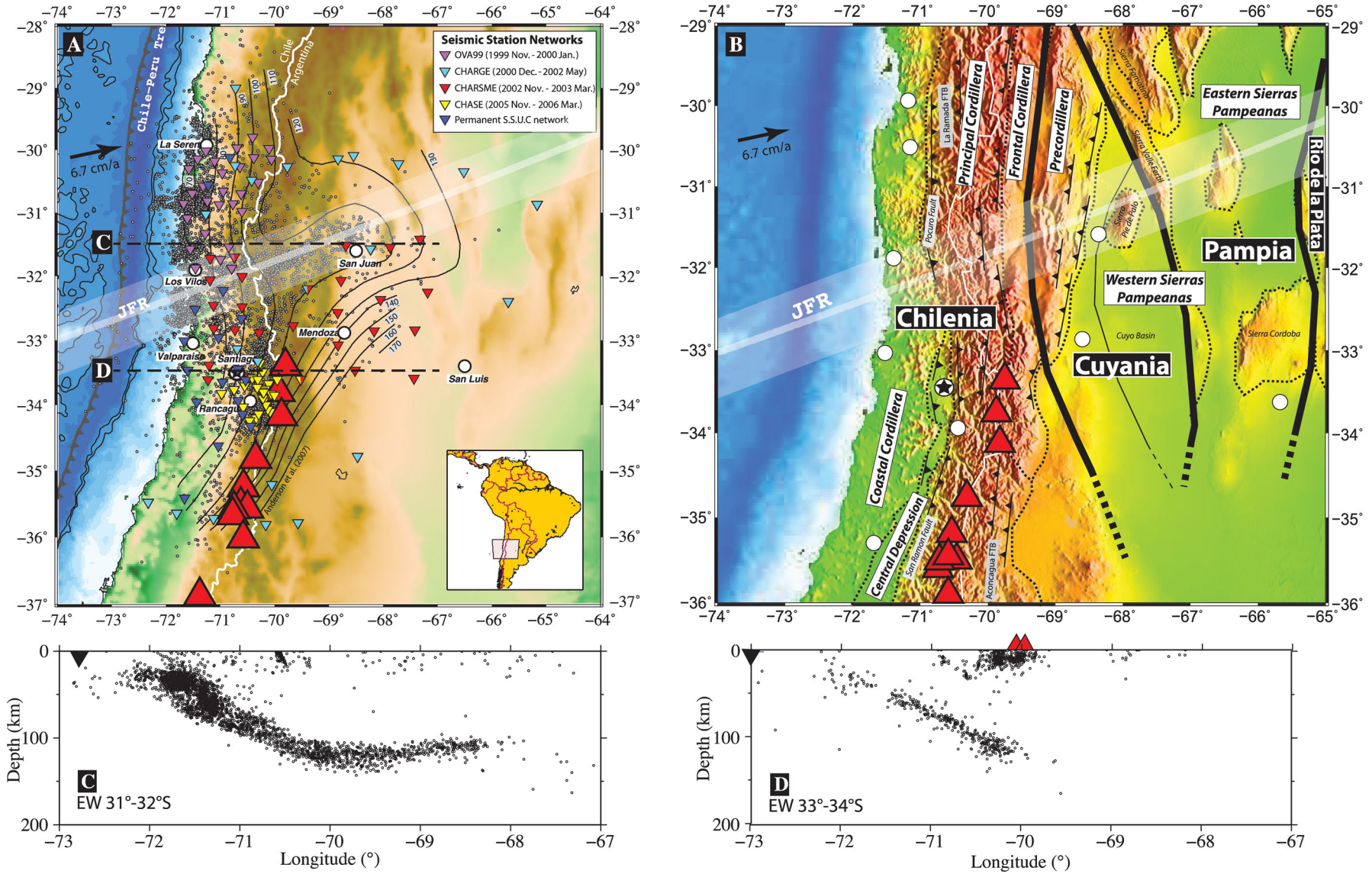

Figure 1. Tectono-seismo-structural-geological context of central Chile and western Argentina, where the Nazca Plate subducts underneath the South American Plate at a rate of 6.7 cm a^{-1} in an N78°E direction (Kendrick *et al.* 2003). (a) Seismological context of the temporary seismic networks (inverted triangles) and the recorded seismicity (small circles). Shown are: active volcanoes (red triangles), main cities (white circles, capital city Santiago with a star), slab contours from Anderson *et al.* (2007), the political border between Chile and Argentina (white line) and the inferred Juan Fernandez Ridge subduction path and width (semi-transparent white line and band, respectively). Inset shows the zone of interest. (b) Tectono-structural-geological context, showing the accreted terranes, major suture zones (thick black lines), geological provinces and their uplifted outcrops (dotted lines), the La Ramada and Aconcagua thrust belts (lines with triangles), and the main cities (white circles, labelled in a). Two vertical EW cross-sections (shown in a) show the recorded seismic activity (black circles) along the flat (c) and normal (d) slab regions; inverted black triangles are the Chile–Peru trench position and red triangles are active volcanoes.

distribution increases (Miranda 2001), (iii) the slab becomes younger (Yáñez & Cembrano 2000), (iv) arc magmatism resumes, (v) the Central Depression valley reappears, (vi) the backarc basement uplift ceases, and the Precordillera and Sierra Pampeanas disappear (Ramos 2009), (vii) the topography decreases from an average elevation of 4500 m (max. elevation is Mount Aconcagua, 6962 m, at ∼70°W/32.5°S) to <2000 m at 38°S, (viii) the crustal thickness decreases from 70 to 35 km (Gilbert *et al.* 2006; Tassara *et al.* 2006; Alvarado *et al.* 2007), (ix) the total lithospheric thickness decreases from 80–100 km (Tassara *et al.* 2006) to 60 km south of 36°S and (x) the rate of seismicity decreases in the backarc region, but increases along the active volcanic arc (Barrientos *et al.* 2004).

Three major terrane accretions have impacted the western proto-Gondwana margin (named here the Rio de la Plata craton) over the past 600 Ma, strongly influencing the structure and tectonic evolution of central Chile (Ramos *et al.* 1986; Ramos *et al.* 2002; Alvarado & Ramos 2011). These terranes have various provenances, compositions and ages, and consist in (Fig. 1b): (i) the para-autochthonous Pampia terrane, amalgamated at ∼530–515 Ma, (ii) the allochthonous Cuyania terrane, accreted at ∼460 Ma and (iii) the allochthonous Chilenia terrane (its existence is still debated), added at ∼420–315 Ma. The Chilenia terrane is believed to compose the Andean basement and part of the forearc crust (Ramos 2004). At the surface, suture zones, characterized by narrow ophiolitic belts today representing major shear zones, separate each terrane and control the region's neotectonic deformation style (Ramos *et al.* 2002) by influencing the thick-skinned Sierra Pampeanas basement cored uplift up to ∼800 km away from the trench (Fig. 1b; Ramos *et al.* 2002; Alvarado *et al.* 2009). However, these terrane boundaries have never been mapped at depth, and the composition of the Andean basement remains enigmatic. Also associated with flat subduction, similar thick-skinned backarc deformation along old sutures (Litherland & Aspden 1992; Gilbert *et al.* 2007), tectonic setting and morphology as in central Chile are observed above the modern Peruvian flat slab (James & Snoke 1994) and in the Laramide Province of western USA which has since been linked to an ancient flat slab episode of the Farallon Plate (Jordan & Allmendinger 1986; DeCelles 2004). Hence, the central Chilean flat subduction is considered a modern analogue of the Rocky Mountain Laramide Province.

3 SEISMIC DATA

3.1 Seismic campaigns

Our seismic tomography inversion is based on passive local earthquakes ($0.5 < M_L < 5.5$) recorded by four temporary seismic campaigns (Fig. 1a):

(1) OVA99: 37 short-period three-component receivers, ∼30 km apart, recorded continuously at a sampling rate of 125 Hz, from 1999 mid-November to 2000 mid-January.

(2) CHARGE (Chile-Argentina Geophysical Experiment, Fromm *et al.* 2004; Wagner *et al.* 2005): 22 broad-band seismometers deployed from 2000 December to 2002 May mainly along two profiles (30°S and 36°S) and some in between, and recorded continuously at a 40-Hz sampling rate.

(3) CHARSME (CHile ARgentina Seismological Measurement Experiment): 29 portable broad-band three-component seismometers recorded continuously at a sampling rate of 125 Hz from mid-November to 2002 March.

(4) CHASE (CHile-Argentina Seismic Experiment): 14 broad-band and 12 short-period seismometers recorded continuously at a sampling rate 125 Hz from 2005 mid-November to 2006 March, and focused in the Santiago area.

Earthquakes recorded by 15 permanent seismic stations from the Chilean Seismological Service (University of Chile, dark blue inverted triangles in Fig. 1a) were added to increase receptor coverage and to improve hypocentre determination near coastal areas.

The OVA99, CHARSME and CHASE networks were installed and maintained by collaboration between GéoAzur and the IRD ('Institut de Recherche pour le Développement') in France, and the Geophysical Department of the University of Chile in Santiago.

3.2 1-D reference model and event selection criteria

The combination of hypocentre relocation, 3-D ray tracing and velocity inversion makes the tomographic problem non-linear, with the danger of ending up in a local minimum; hence, the importance of using a 1-D model close to the (likely) reality is crucial. All events were therefore consistently located using programme Hypoinverse (Klein 2000) and a 1-D velocity model which best fits, in a least-squares sense, data from both active and passive sources from the region. The 1-D velocity model was then adjusted below 20-km depth using programme Velest (Kissling *et al.* 1994). The chosen model consists of 17 layers, with an average Vp/Vs ratio of 1.76, extrapolated to 215-km depth for the inversion (Fig. 2, black line). Our 1-D background model is similar to that used by Haberland

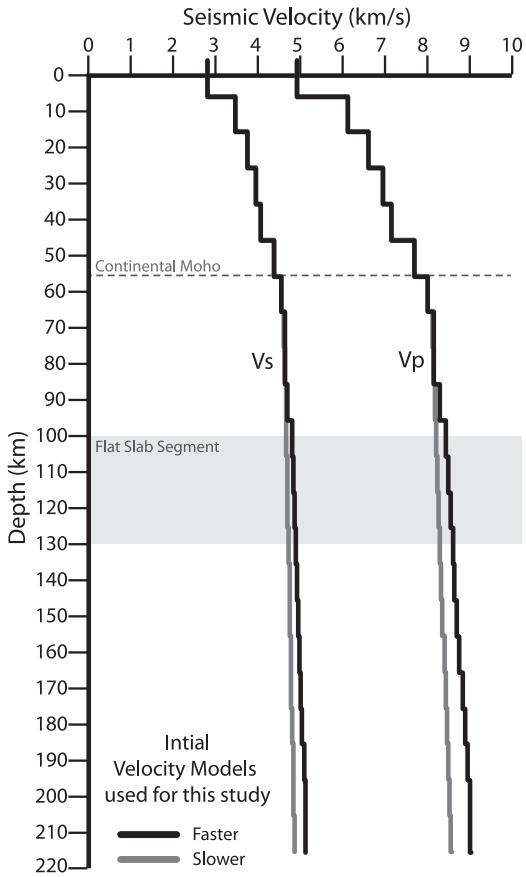

Figure 2. 1-D initial velocity models for *P* and *S* waves used for our tomography inversion, and calculated for the region. For more information, refer to Section 3 in the text.

et al. (2006) for the Maule region, and to Sanchez *et al.*'s (2013) (INPRES) at mantle depths for western Argentina, although the crustal velocities in the latter study are higher between 20 and 55-km depth (Fig. 2). In comparison, the IASPEI-91 1-D velocity model (Kennett & Engdahl 1991) used in Wagner *et al.*'s (2005) study, differs greatly from all regional models, with slower seismic velocities, because it represents average global velocities and considers a Moho at 35-km depth, whereas it is measured at 55–70-km depth in central Chile (see Fig. 2). The high seismic velocities for this region can also be attributed to the cooler environment associated with flat subduction.

To ensure stability and reliability of our tomography results, we selected only the highest quality events from our event catalogue, with the following selection criteria for *P* and *S* waves, respectively: (i) maximum error of computed traveltime residual of ±0.25 and ±0.4 s, (ii) maximum pick quality index of 2 and 3 (0: excellent, 4: discarded), (iii) maximum hypocentre uncertainty of 5 km in all directions, (iv) maximum rms misfit of <0.6 s ($\sqrt{R_i^2/N}$, where R_i is the traveltime residual at station *i*, and *N* the number of observations per event), (v) minimum eight and four station observations and (vi) azimuthal gaps of ≤300°, to maximize the number of offshore events taken into account in order to image the Chilean margin. Finally, we retain a total of 3770 events (55 128 *P*- and 54 889 *S*-wave arrival times) for the inversion process.

A catalogue of relocated earthquakes can be obtained from GéoAzur by contacting Tony Monfret at monfret@geoazur.unice.fr.

4 SEISMIC TOMOGRAPHY: METHOD

4.1 3-D inversion

Our data represent onset times and are interpreted using ray theory. We apply the tomography code TLR3 (Latorre *et al.* 2004; Monteiller *et al.* 2005) to obtain 3-D *P*- and *S*-wave velocity models, from which we then calculated a *Vp*/*Vs* model. Source–receiver ray trajectories are calculated using the finite-difference algorithm from Podvin & Lecomte (1991) within a fine grid model of mesh size 2 × 2 × 2 km, to enable ray path smoothness. Our inversion model is discretized into a coarser regular grid of mesh size 40 × 40 × 10 km, representing total dimensions of 960 × 840 × 220 km (*x*, *y*, *z*, respectively), in which body wave traveltimes are calculated. The 3-D velocity structure is progressively retrieved through a set of iterations which solve for small velocity perturbations in order to linearize the problem and reduce computational time constraints caused by the large data set. Hypocentres are simultaneously relocated at each step. The starting iteration involves the initial 1-D velocity model (Fig. 2, black line) and its relocated seismicity. Values for damping and weight ratio (*Cp*/*Cs*) of *P*- and *S*-wave traveltimes were adjusted separately by fixing one parameter at a time and allowing the other to vary, in order to obtain those that minimize the solution rms misfit. The parameters in TLR3 that led to best results were a damping value of 0.7 and a *Cp*/*Cs* value of 0.5. Mesh spacing and final velocity model robustness were examined using the checkerboard and spike tests. The well-resolved regions of the model have a spatial resolution representative of the mesh spacing used, and represent areas where the seismicity is densest.

4.2 Final solution model quality assessment

In this study, the inversion of traveltimes is performed using the LSQR algorithm (Paige & Saunders 1982), which does not provide a resolution matrix. *A posteriori*, we assessed the resolution quality of our final model using the ray density distribution, and the harmonic checkerboard (Fig. 3) and spike sensitivity tests (Fig. 4). The latter two examine the possible artefacts introduced in the model space during the inversion process, by assessing the restoration of amplitude, shape and extent of synthetic velocity perturbations. Our checkerboard tests considered three different mesh spacings, 80 × 80 × 20, 40 × 40 × 10 and 30 × 30 × 10 km, with the latter two offering the best resolution solutions. We chose to retain and to base our discussion on the mesh spacing of 40 × 40 × 10 km, because 80 × 80 × 20 km offers a too coarse and poorer rms misfit, and 30 × 30 × 10 km, although well resolved, brings a too detailed and complex image pattern. We then constructed a synthetic spike test model to evaluate the characteristics (perturbation sign, location and geometry) of the most dominant features obtained in our final velocity model (red and blue box contours in Fig. 4).

As shown by the checkerboard and spike tests, the regions closest to the subduction interface, where ray densities are highest, are best resolved. The overriding lithosphere is well resolved above the flat and normal slabs, with a good recovery of both amplitudes and geometry of the synthetic input model. Also, the upper part of the oceanic lithosphere, assumed to be represented by the thick seismogenic zone (∼20–30 km from the top of the slab) is well recovered throughout the region. On the other hand, though our spike test indicates that the backarc regions over the flat and normal slabs (the Cuyania terrane) are well resolved, our checkerboard test shows leakage from less well-resolved voxels. A careful interpretation of our backarc seismic velocities is required.

The checkerboard tests (Fig. 3) give a broad indication where the model is best resolved, the regions closest to the subduction interface, where ray densities are highest, and where resolution is lacking. For this reason, the backarc region will be discussed with caution. The accuracy of absolute velocities is important for judging the reliability of petrological interpretations. In Fig. 4, we therefore test the amplitude accuracy for realistic units. We find that the solution reproduces the input amplitudes of these structures to better than 90 per cent, that is, an absolute accuracy of better than 50 m s^{-1}.

5 SEISMIC TOMOGRAPHY: RESULTS

5.1 The forearc crust

The forearc crust (Coastal Cordillera), between 5 and 25-km depth, is generally characterized everywhere by fast seismic velocities and low *Vp*/*Vs* ratios, which are limited to the east by the western Andean La Ramada–Aconcagua thrust belt, forming the boundary between the Coastal and Principal Cordilleras (Fig. 5a). *Vp* is constant throughout the region (6.2 km s^{-1}). However, at latitudes <32°S (in the flat slab region), between 0 and 10-km depth, the forearc exhibits unusually low *Vp*/*Vs* ratios of 1.69–1.73 due to increased *Vs* values (3.6–3.7 km s^{-1}) peaking in the Punitaqui region (Figs 5a and 6b). In comparison, south of 32°S (above the subducting JFR and in the normal slab region), *Vs* is slower (3.4–3.5 km s^{-1}) and *Vp*/*Vs* values are higher (1.74–1.76). This anomaly is of difficult interpretation; however we suggest several explanations for its nature and presence in the flat slab region.

Throughout the region, below 10-km depth, is a 10-km thick layer of reduced *Vp* and *Vs*, and higher *Vp*/*Vs* ratios (1.78) (Figs 6a and b), connecting the plate interface with the Principal Cordillera, and

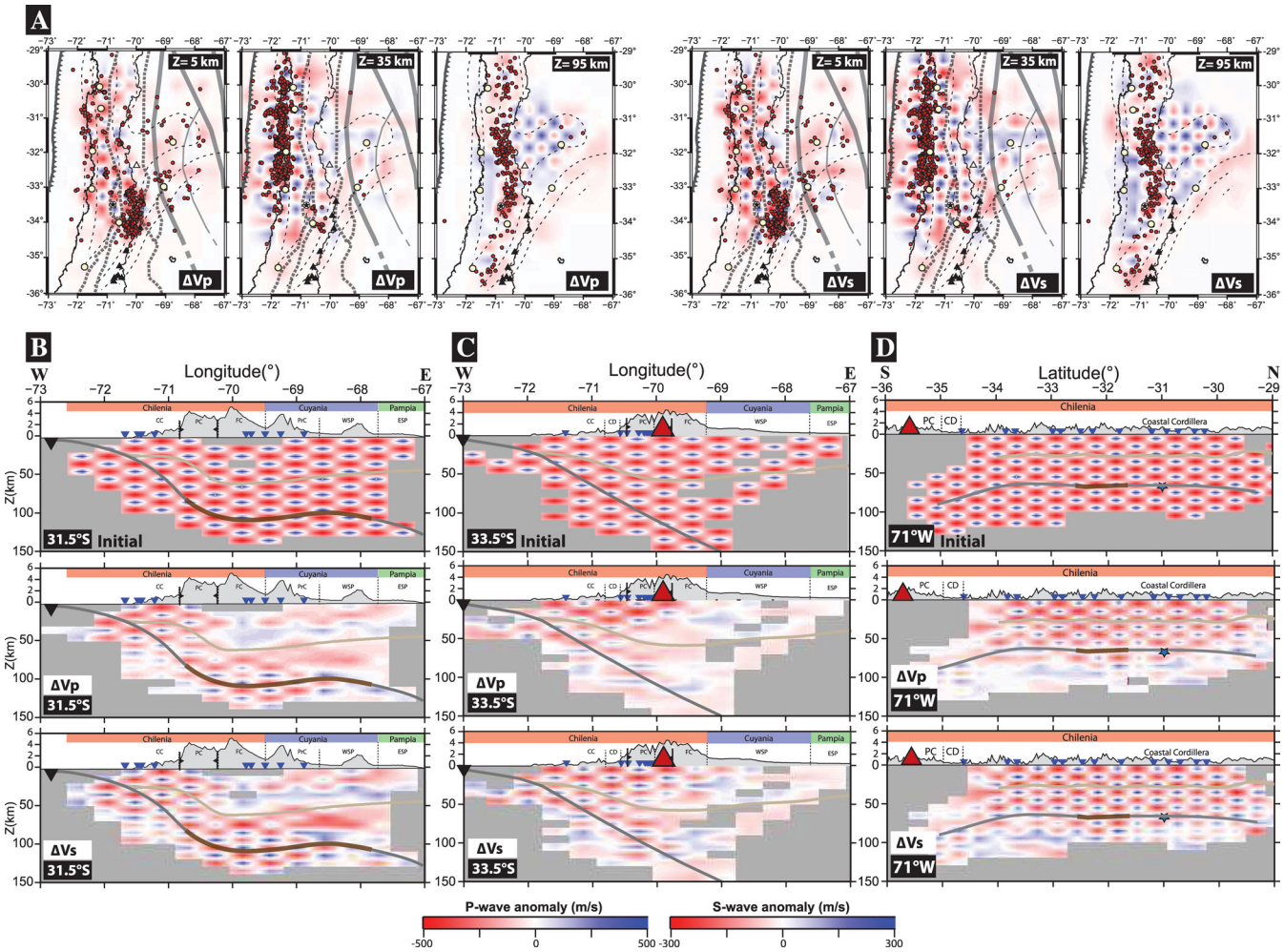

Figure 3. Checkerboard test results for our final *P*- and *S*-wave velocity models. (a) Plan view at 5, 35 and 95-km depths. (b) and (c) Vertical EW cross-sections along the flat and normal slab regions. (d) Vertical NS cross-section along the Cuyania terrain in the backarc region at 68.5°W. The initial synthetic velocity perturbations for *P*and *S* waves are 500 and 300 m s^{-1}, respectively. The horizontal and vertical node spacings are 40 and 10 km, respectively. Grey shaded cells reflect areas of poor ray density, determined by fixing a certain threshold value for the total ray length crossed in each cell. Also shown are: the slab geometry (isocontour lines from Anderson *et al.* 2007), the location of active volcanoes (red triangles), the seismic stations (inverted blue triangles), the inferred slab interface based on our relocated seismicity (dark grey line), the expected location of the subducted Juan Fernandez Ridge material (thick brow line segment), the continental Moho from seismic (Fromm *et al.* 2004) and gravity (Tassara *et al.* 2006) studies, the topography and the geological and tectonic terrane boundaries (thick dotted and solid lines, respectively). CC, Coastal Cordillera; PC, Principal Cordillera; FC, Frontal Cordillera; CD, Central Depression valley; PrC, Precordillera; WSP, Western Sierras Pampeanas; ESP, Eastern Sierras Pampeanas.

suggesting a possible zone of slab fluid concentration, as we discuss in the next section.

Two other areas of distinctly reduced seismic velocities and high *Vp*/*Vs* ratios occur near the surface, above the normal slab, with unknown origins: (1) northeast of Valparaiso city (70°W/33°S), down to ∼25-km depth, spatially associated with a cluster of seismicity (Fig. 5a); and (2) directly beneath Rancagua city (∼70.5°W/34°S), down to only ∼10-km depth, displaying a *Vp*/*Vs* ratio that is by far the highest in the region (1.86). These high *Vp*/*Vs* ratios could suggest important fluid (O'Connell & Budiansky 1974) or (but less likely) melt (Watanabe 1993) concentrations in the rock, with a possible thermal influence inherited from the relatively recent Andean magmatism (4–9 Ma, also responsible for the El Teniente and Rio Blanco-Los Bronces porphyry copper deposits) and currently active volcanism in the Eastern Principal Cordillera (Farías *et al.* 2010). In both cases, it may be of interest to reevaluate the local seismic hazard at these localities, given these new observations.

5.2 The main Andean crust

The entire Andean crust, and particularly the Principal Cordillera, is characterized by significantly reduced seismic velocities and moderately high *Vp*/*Vs* ratios (∼1.78–1.79) (Figs 5a, b, and 6). Beneath the active and ancient volcanic arcs, down to 25–30-km depth, the Principal Cordillera exhibits the slowest seismic velocities together with moderately high *Vp*/*Vs* ratios (1.78–1.80) (Fig. 5b). The orientation (NNW-trending) and dimension (∼100-km wide) of this anomaly mimic those of the La Ramada–Aconcagua deformation belt. South of 33°S and ∼50-km west of the active volcanic arc, the seismic velocities in the Principal Cordillera are slower and associated with intense and deep seismicity (Figs 5a and b), related to arc volcanism.

On the other hand, the Frontal Cordillera shows less reduced seismic velocities, with the exception of the region between 33°S and 34°S, bounded to the east by the Cuyania–Chilenia suture zone.

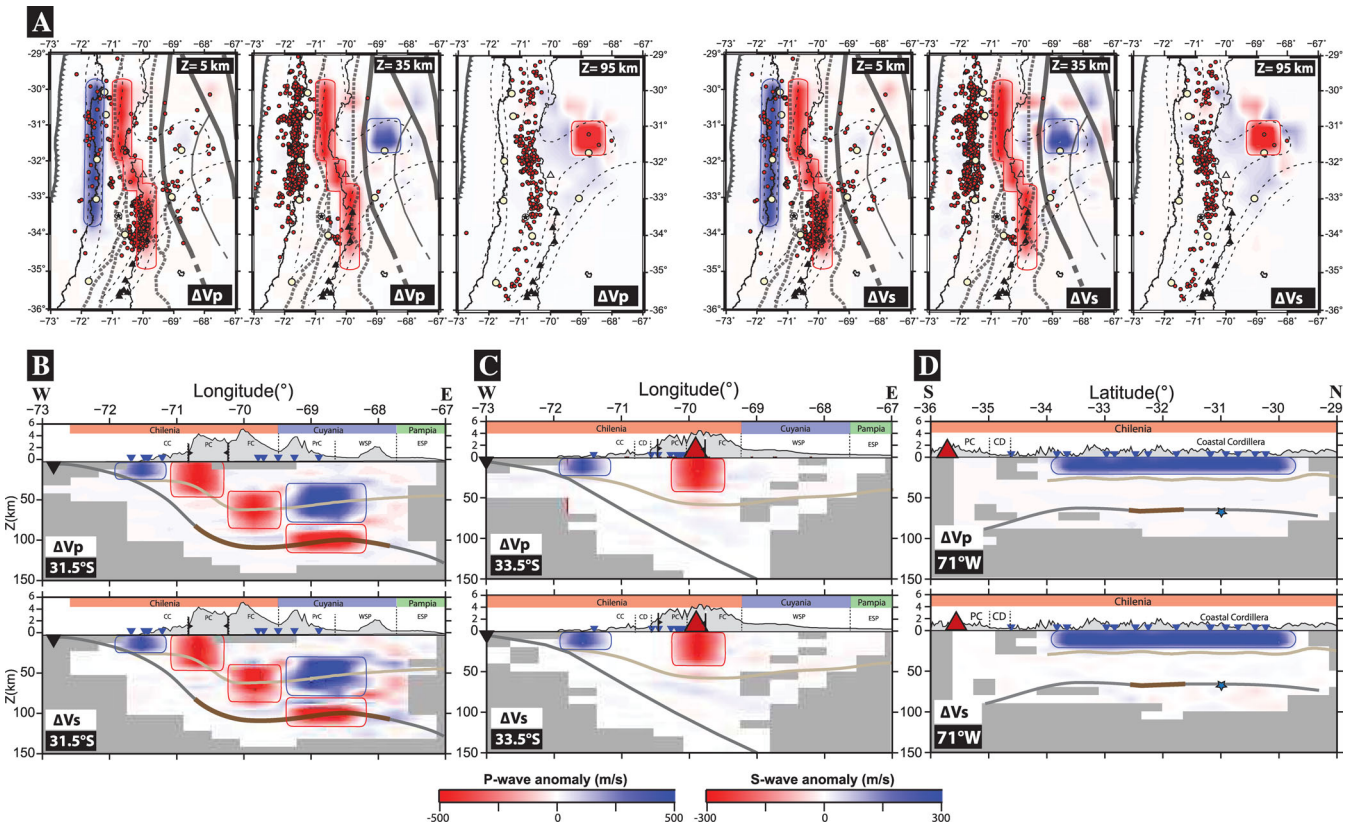

Figure 4. Spike test results for our final *P*- and *S*-wave velocity models. (a) Plan view at 5, 35 and 95-km depths. (b and c) Vertical EW cross-sections along the flat and normal slab regions. (d) Vertical NS cross-section along the Cuyania terrain in the backarc region at 68.5°W. Blue (positive) and red (negative) outlined boxes shown the initial velocity perturbations imposed on our final velocity inversion model of amplitudes ±500 m s^{-1}. The regions closest to the highest seismicity density are well resolved with almost not distortions, however, the backarc region is less well constrained by the ray coverage, leading to some horizontal smearing, mostly in the continental mantle below Cuyania. Figure legend as in Fig. 3.

Here, *Vp* and *Vs* are as low as in the Principal Cordillera and the *Vp*/*Vs* ratios are locally higher (Fig. 5a), suggesting a similar cause as the Principal Cordillera, such as structural damage, at least at shallow depths.

At deeper crustal levels (>30 km), this slow velocity anomaly, originating at the surface of the Principal Cordillera, propagates downwards and eastwards into the Andean crustal root (beneath the Frontal Cordillera) and into the sublithospheric mantle towards the slab interface beneath Cuyania (68.5°W, Figs 6a and b). This pattern is further detailed in the 'continental mantle' subsection.

The seismic continental Moho (Fromm *et al.* 2004) appears to follow the isocontour lines *Vp* ∼8.0 km s^{-1} and *Vs* ∼4.5 km s^{-1} (Fig. 6).

5.3 The backarc crust

Our resolution of the backarc region is limited, especially above the normal slab (>33°S), as shown by our checkerboard and spike tests (Section 4, Figs 3 and 4). Nevertheless, it is reasonably resolved above the flat slab due to the higher ray coverage produced by the flat slab's seismicity, and one can clearly identify the Cuyania terrane (Precordillera and western Sierra Pampeanas) as a fast seismic anomaly, bounded on each side by suture zones. The first 75–80 km of the Cuyania lithospheric column show slightly faster *Vp* and *Vs* values and lower *Vp*/*Vs* ratios (1.70–1.74) (Figs 5 and 6a, b and d) than the surrounding lithosphere. This observation differs from previous studies, which characterize it with higher *Vp*/*Vs* values (>1.80) based on 1-D velocity forward modelling (Gilbert *et al.* 2006; Alvarado *et al.* 2007). However, our relatively poor resolution for this region forces caution in our interpretation.

5.4 The continental mantle

Throughout the region, the continental mantle exhibits reduced *Vp* and *Vs* values between 50 and 60-km depth and higher *Vp*/*Vs* ratios (1.77–1.78) than the surrounding mantle (Figs 6a and c). Overall, a comparison of the continental mantle above the flat and normal slabs yields little change. However, a notable difference is the existence of a very low *Vp*/*Vs* anomaly (1.70–1.74) in the mantle wedge corner above the flat slab (at latitudes <32°S), between 35 and 50-km depth (Figs 5b and 6b). Here, *Vs* increases substantially (4.0–4.4 km s^{-1}) compared to the region above the normal slab (3.9–4.1 km s^{-1}), whereas *Vp* remains the same (6.9–7.7 km s^{-1}), analogous to the shallow forearc anomaly directly above it.

Below 70-km depth, the continental mantle above the flat slab is characterized by relatively high *Vp* (8.0–8.5 km s^{-1}) and *Vs* (4.5–4.8 km s^{-1}), relatively low *Vp*/*Vs* ratios (1.75–1.77), reflecting the regional low temperature distribution, and containing localized patches of higher *Vp*/*Vs* values (1.79), which may indicate slight hydration (Figs 6a and b).

Beneath the Frontal Cordillera, the mantle exhibits low seismic velocities (Figs 6a and b), correlated with *P*-wave attenuation (Fig. 7a; Deshayes 2008). This anomaly appears to extend deeper eastwards towards the flat slab's interface at 68.5°W, directly

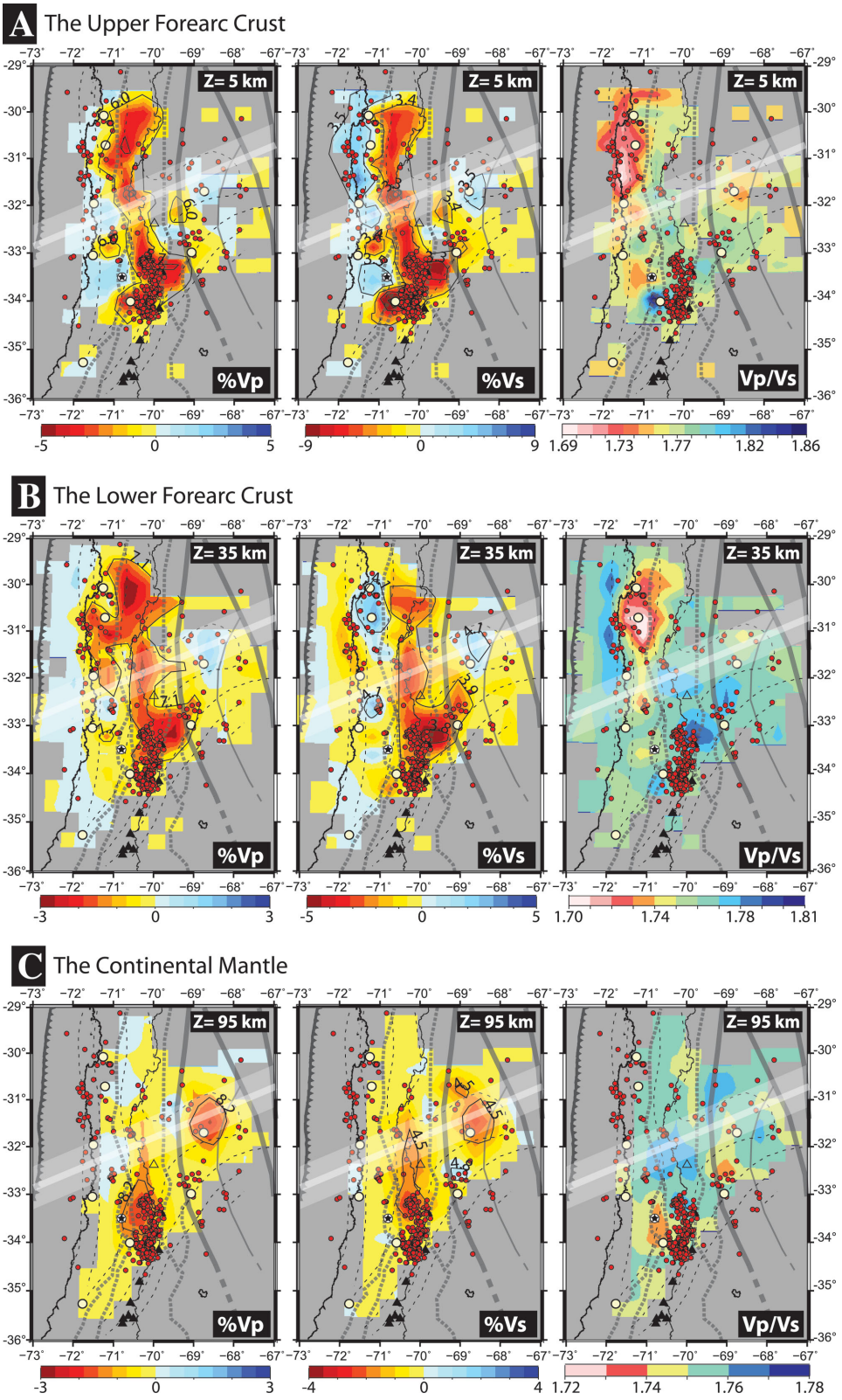

Figure 5. Plan view of our final 3-D velocity model perturbations for *P* and *S* waves, relative to our initial velocity model (black line in Fig. 2) at depths (a) 5 km, (b) 35 km and (c) 95 km, cross-cutting the shallow forearc, deeper forearc and continental mantle seismic anomalies, respectively (details in text). Contour lines are the absolute *P*- and *S*-wave velocities. Red dots are the seismicity at these depth slices. Small empty triangle at the centre indicates the location of the Aconcagua highest peak of the region (6962 m). Figure legend as in Fig. 3.

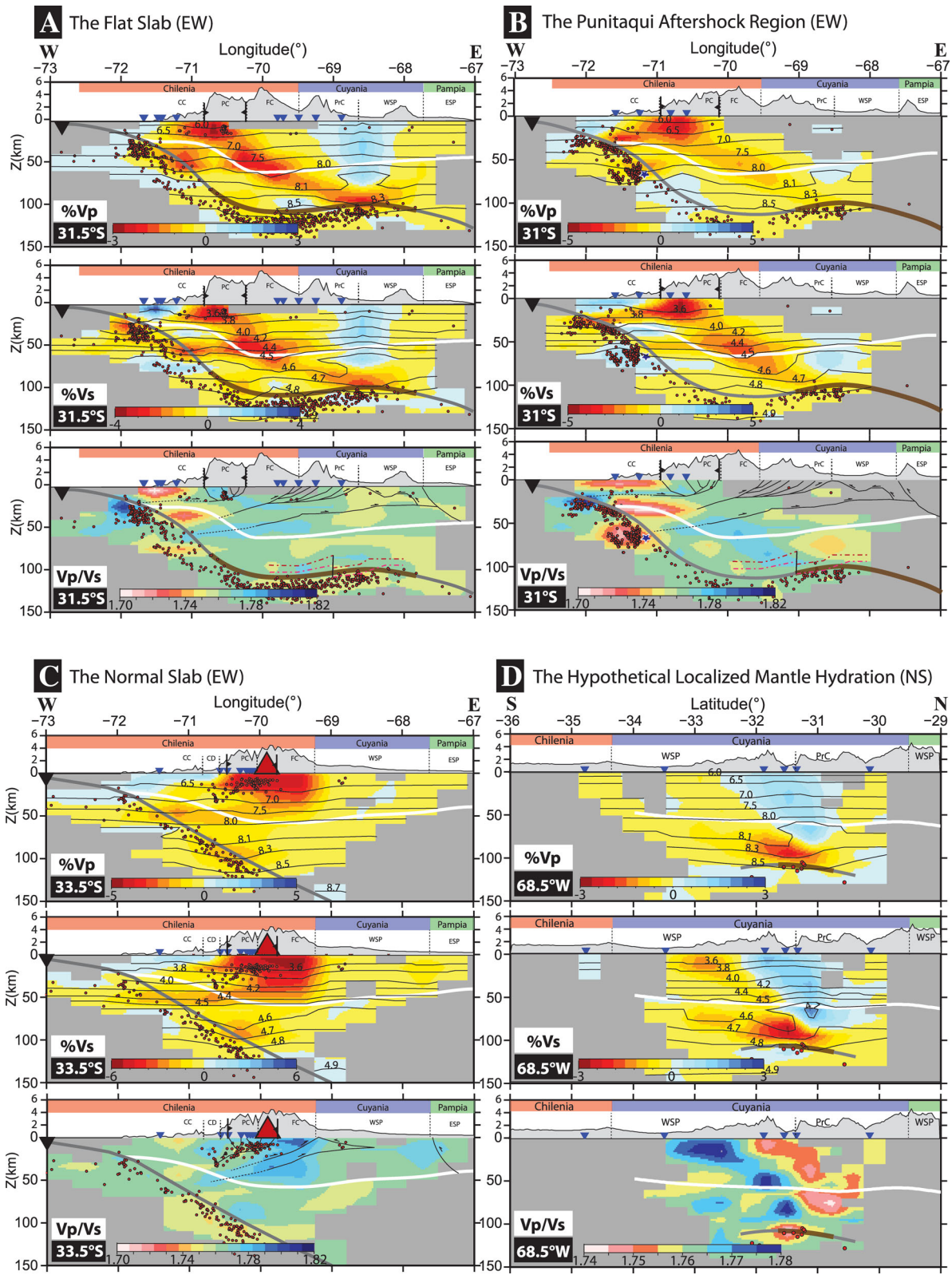

Figure 6. Vertical cross-sections of our final 3-D velocity model for *P* and *S* waves, relative to our initial velocity model (black line in Fig. 2), describing EW cross-sections along the flat slab regions where the JFR subducts (a) and across the Punitaqui aftershock area (b), the normal slab region (c) and an NS cross-section across the Cuyania lithosphere (d), showing possible mantle hydration. Contour lines are absolute seismic velocities. Red dots represent the seismic events used for our tomography (see Section 3 for details). Back lines outline the tectonic models for the Andes and backarc regions from Farías *et al.* (2010) and Ramos *et al.* (2002), respectively, and dotted lines show our inferred extensions of major basement shear zones (hypothetical), correlating well with regions of higher *Vp*/*Vs* ratios. Dotted dark red and pink lines describe Gans *et al.*'s (2011) model, based on receiver function analysis, for the flat slab interface and Moho, with speculative vertical offset (vertical black line) along the flat slab. Figure legend as in Fig. 3.

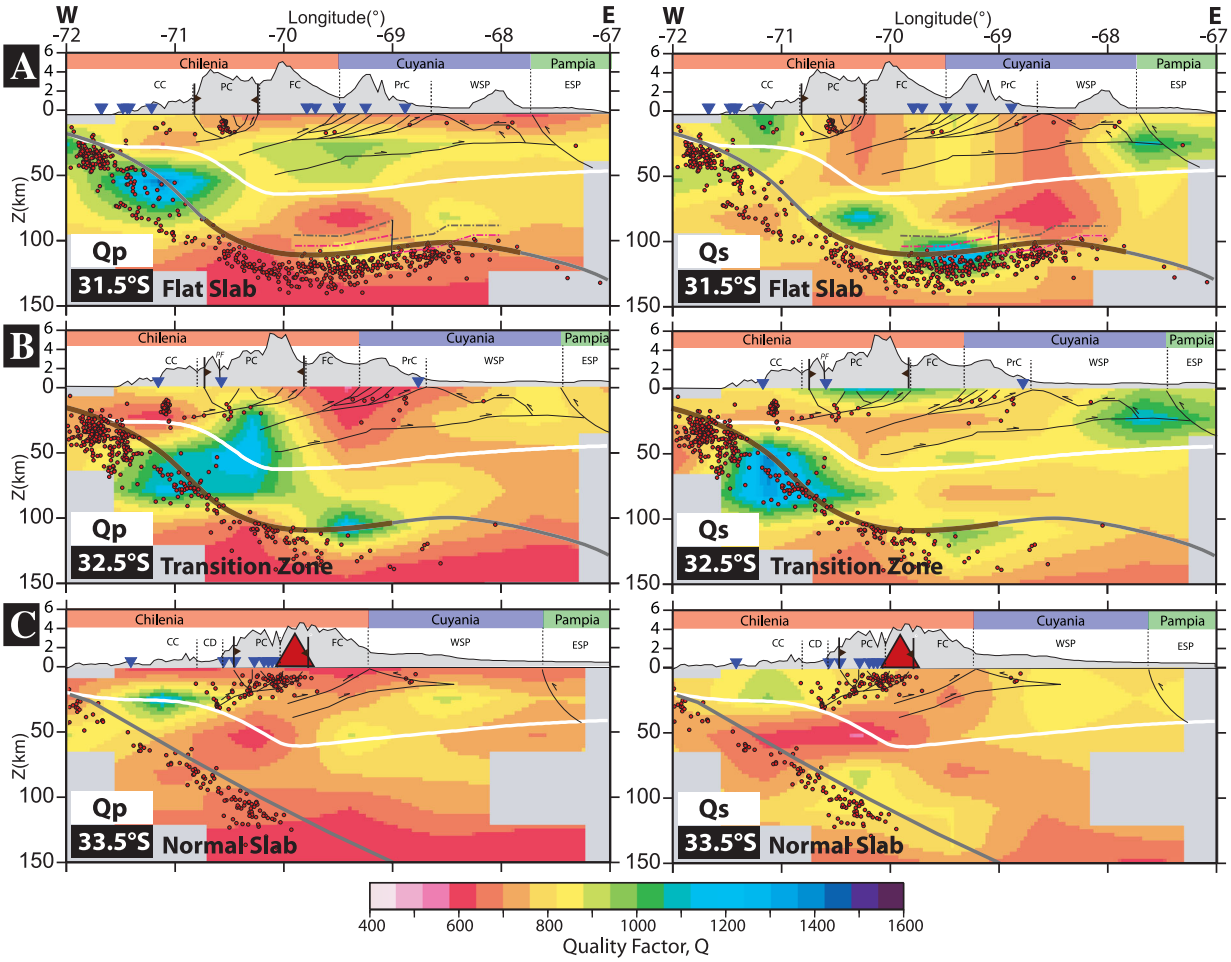

Figure 7. Seismic attenuation models for *P* and *S* waves calculated by Deshayes (2008) for the region along the (a) flat slab, (b) transition and (c) normal slab regions, using events from the OVA99 and CHARM campaigns. Note that the model is limited at 72°W. Figure legend as in Fig. 3.

beneath the Cuyania terrane (Figs 6a and b), where it forms a 10–20-km thick and ∼1000 km^2 area (Fig. 5c) region of slow seismic velocities, lying directly above the JFR location and at the eastern tip of the flat slab segment, just before resubduction occurs. This thin anomaly, at 95-km depth, exhibits a locally higher *Vp*/*Vs* ratio (1.78) than the surrounding mantle (1.75) (Fig. 6d), as well as being characterized by *S*-wave attenuation (Fig. 7a; Deshayes 2008). We discuss in the next section this anomaly as observed by several independent studies, strongly supporting mantle hydration. The two seismic anomalies in the continental mantle beneath the Frontal Cordillera and the backarc appear physically connected to one another and to the shallow Principal Cordillera crust.

5.5 The subducting plate

In the flat slab region (<32.5°S), the subducting plate down to ∼50-km depth is highly seismogenic, showing strongly reduced seismic velocities and concomitant high *Vp*/*Vs* ratios (1.80–1.82) (Figs 6a and b), suggesting the presence of fluids and dehydration reactions (e.g. Hacker *et al.* 2003b). Below, between 50 and 75-km depth, both *Vp*/*Vs* ratios and the seismic rate of the Double Seismic Zone's upper plane decrease (Fig. 6a), suggesting a change in the slab's rheology.

At 31°S, 71°W and 50–80-km depth, a local seismic anomaly of decreased *Vp* (8.0–8.1 km s^{-1}) and strongly increased *Vs* (4.5–4.7 km s^{-1}) resulting in very low *Vp*/*Vs* ratios (1.70–1.73) exists at intraslab depths, with approximate dimensions 50 × 40 × 25 km (*x*, *y*, *z*). It defines the 1997 Punitaqui (*M*w 7.1) aftershock region (hypocentre shown by the blue star in Fig. 6b). The lowest *Vp*/*Vs* value is located in the interplanar region of the Double Seismic Zone found in this region (Marot *et al.* 2013). This anomaly is possibly linked with a low *P*-wave attenuation anomaly present at 31.5°S (Fig. 7a; Deshayes 2008).

The western part of the flat slab segment (>100 km of depth), between 69°W and 70.5°W, is characterized by higher *Vp* (8.5–8.6 km s^{-1}) and *Vs* (4.8–4.9 km s^{-1}) than its eastern part (8.4–8.5 and 4.7–4.8 km s^{-1}, respectively). This difference is particularly pronounced along the JFR axis (Figs 6a and b). Nevertheless, the *Vp*/*Vs* ratios remain similar and relatively low (1.75–1.77).

In comparison, the normal slab (>33°S) down to 50-km depth is less seismogenic and shows a less pronounced decrease in seismic velocities than the flat slab at these depths, with slightly lower *Vp*/*Vs* ratios (1.76–1.78) (Fig. 6c). Between 50 and 75-km depth, the seismic activity increases and *Vp* decreases, resulting in even lower *Vp*/*Vs* ratios (1.74–1.76) than its shallower counterpart. Below 125–150-km depth, the seismic activity becomes rare.

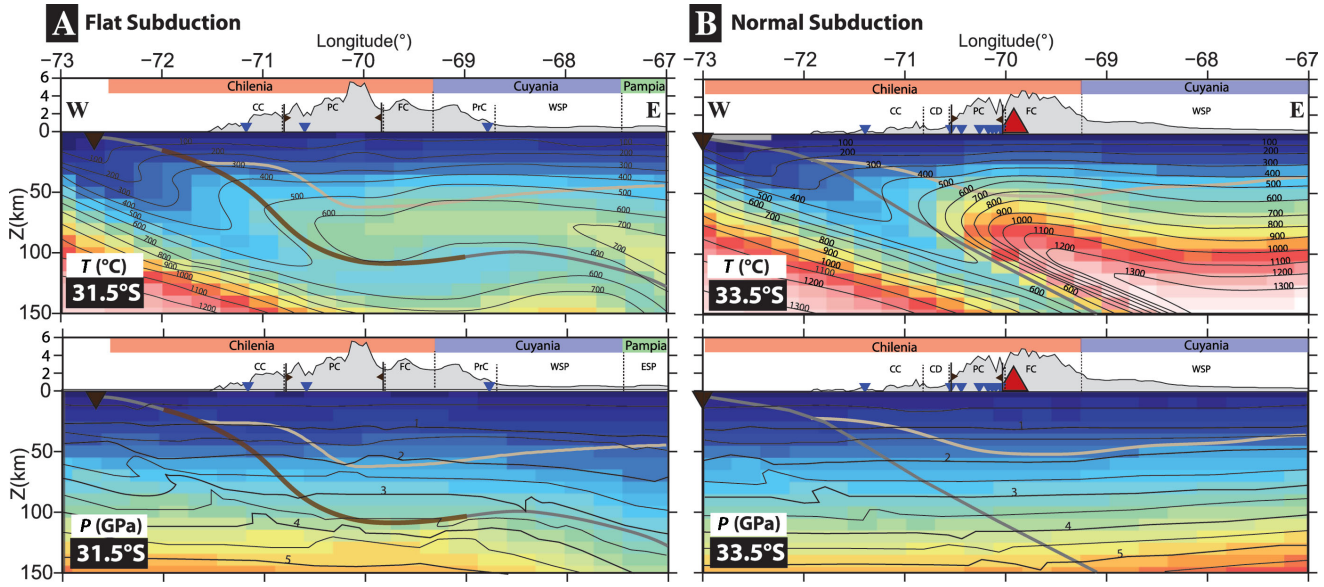

Figure 8. Our final synthetic *P–T* models computed to represent the central Chilean (a) flat and (b) normal slab zones, used for our petrological analysis. See Section 6 for details on the computation method. Isocontour lines define the temperature (*T*) and pressure (*P*). The uncertainty for *T* and *P* are of the order of ±100 °C and ±0.5 GPa, respectively. Figure legend as in Fig. 3.

6 PETROLOGICAL ANALYSIS

6.1 Estimation of the *P–T* conditions

In order to correlate our seismic velocities with those predicted for rock types likely to constitute the lithosphere, we first need to estimate the appropriate pressure (*P*) and temperature (*T*) conditions at depth. A conventional approach consists in defining kinematical models of subduction that calculate a temperature field equilibrated with the velocity of subduction (e.g. Springer 1999; Gutscher *et al.* 2000), and assuming lithostatic pressure. Here instead, we chose to estimate the *P–T* field along two vertical cross-sections representing the central Chilean flat (31.5°S) and normal (33.5°S) subduction zones, with a thermomechanical model that can account for some tectonic overpressure as well as shear heating along the plate interface. The plane-strain finite differences code Parovoz (Poliakov & Podladchikov 1992) was used, which is based on the FLAC method (Fast Lagrangian Analysis of Continuum, Cundall & Board 1988). This code has been used in a variety of geodynamic contexts (e.g. Gerbault *et al.* 2009, and references therein), and solves the equations of motion and heat transfer explicitly in a time-marching scheme, with self-consistent elasto-visco-plastic temperature-dependent rheologies (details in Gerbault *et al.* 2009).

Our aim here is not to reproduce the progressive formation of a flat subduction, for which mechanical causes are still subject of debate (e.g. Van Hunen *et al.* 2004; Gerbault *et al.* 2009; Martinod *et al.* 2010, 2013; Cerpa *et al.* 2014). Instead, we determine thermomechanical parameters for which the present-day geometry is stable over several millions of years, a timing of the order of the geological record (e.g. Haschke *et al.* 2006) and appropriate to generate the observed seismic velocities. Therefore, given an applied convergence rate of 7.5 cm a^{-1} (estimated for the past 4.9 Ma, Somoza & Ghidella 2005), the computational time is chosen to span ∼4 Ma, during which the geometrical setup should evolve relatively little (so that external changes in kinematical and thermal initial conditions can be neglected at this timescale as well as internal phase changes, Gerbault *et al.* 2009).

The synthetic modelled domain is first subdivided into several rheological units describing the different parts of the continental and oceanic lithospheres at present day. The geometries of these units are constructed based on our catalogue of hypocentre distribution at depth. The initial temperature distributions are evaluated to best-fitting estimates by Tassara *et al.* (2006), as well as surface heat flow data by Hamza & Muñoz (1996). Therefore, we assume effective thermal ages of the oceanic and continental lithospheres of 35 and 200 Ma, respectively, and a lithosphere/asthenosphere boundary (LAB, defined by the 1350 °C isotherm) set at 120 and 150-km depths for the normal- and flat dipping slabs, respectively. The thermal effect of the magmatic arc in the normal-dipping slab section is simulated with a Gaussian thermal anomaly centred above the position of the slab at depth 100 km, whereas it is negligible in the flat slab section. Other thermal parameters can be found in Gerbault *et al.* (2009).

In order to model a consistent mechanical behaviour, we assign power-law creep wet olivine parameters for the lithospheric mantle in the normal-dipping subduction section, and in the flat slab section, dry olivine parameters. To concentrate crustal deformation where seismicity and crustal thickening are observed, the magmatic arc domain in the normal-dipping section was assumed to behave as weak granite, whereas the area corresponding to the Cuyania terrane, in the flat slab section, was assigned harder plagioclase parameters (see details in Gerbault *et al.* 2009, and Ranalli 1995 for rheological parameters). We have chosen layer-constant densities for the crustal and mantle units, similar to those obtained by the gravity modelling of Tassara *et al.* (2006). We also assumed constant elastic properties, as these parameters do not significantly affect the deformation and stress fields over a 4-Ma timescale considered here. Nevertheless, compositional changes in the elastic and density properties affect seismic velocities. For instance, Afonso *et al.* (2010) showed that for temperatures below ∼900 °C and in the absence of garnet, a change of ∼15 vol% olivine in a rock produces equivalent changes in *Vp* and *Vs* to a temperature change of 100 °C. Considering this effect, together with uncertainties inherent to synthetic models and

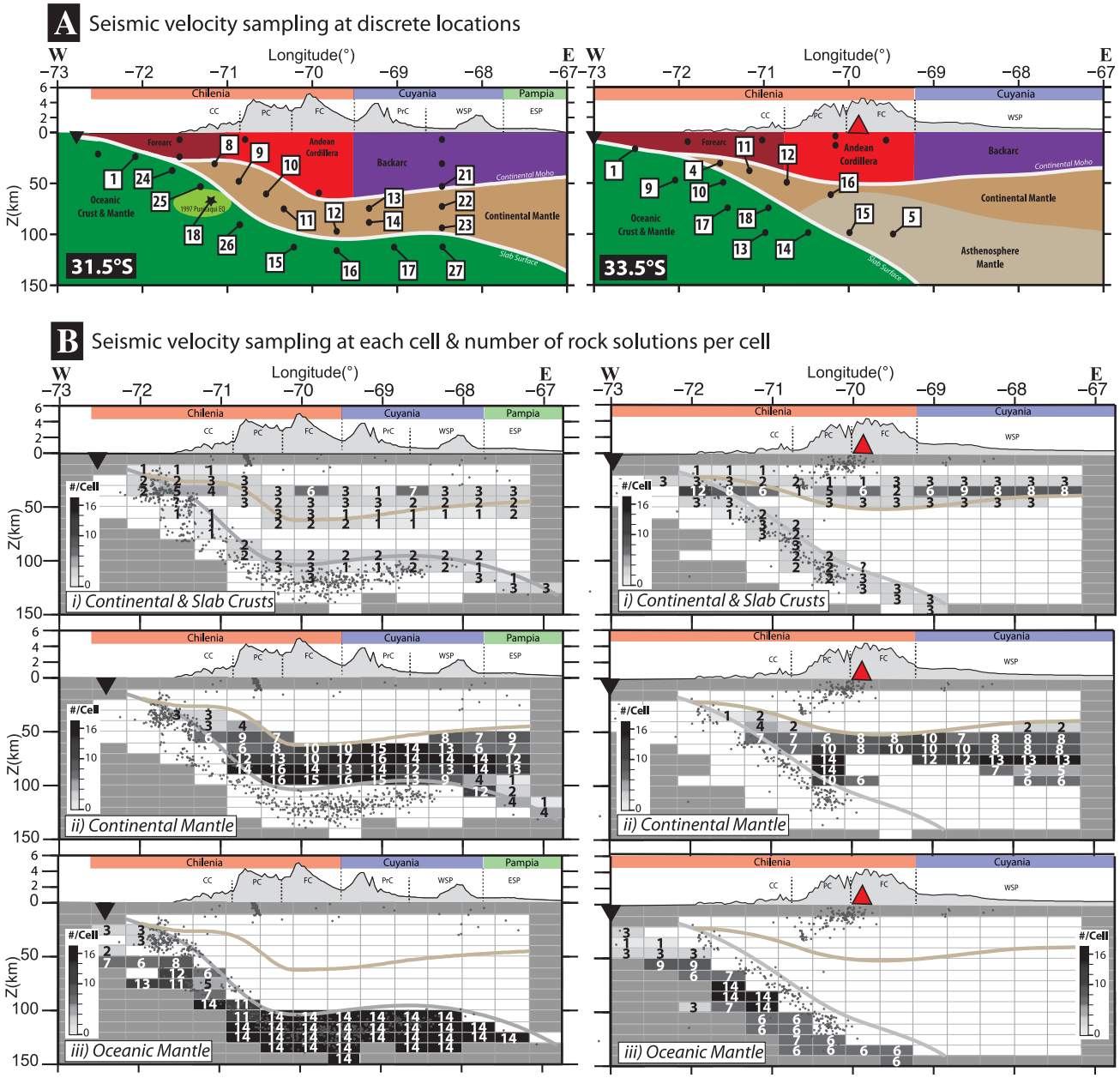

Figure 9. Areas sampled for our petrological analysis, whereby our absolute seismic velocities for the flat (left-hand side) and normal (right-hand side) subduction regions are compared with predicted rock seismic velocities computed using the Hacker & Abers (2004) worksheet and rock composition database. (a) Discrete and precise locations of interest. Numbers make reference to Fig. 11. (b) Within each cell (dimensions are 40 × 10 km). Numbers and colour shading refer to the number of rock solutions found matching our seismic velocities observed in each cell. Figure legend as in Fig. 3.

the effects of shear heating and tectonic pressure, we assume a permissive range of uncertainty in the resulting modelled *P*--*T* values of ±100 °C and ±0.5 GPa. The two synthetic *P*–*T* profiles obtained for the normal-dipping and flat slab sections are shown in Fig. 8, and can now be used as input data for our petrological analysis.

6.2 Petrological modelling

For each cell (Fig. 9b) and for several discrete sites (Fig. 9a) in our 2-D representative cross-sections of the central Chilean flat (31.5°S) and normal (33.5°S) subduction zones, we analysed which rock types matched best our calculated seismic velocities for (i) the forearc crust, (ii) the continental lower crust, (iii) the continental mantle and (iv) the resolved upper slab regions. We based our analysis on experimentally measured isotropic seismic properties of mafic and ultramafic rock compositions, representative of subduction zones (Hacker *et al.* 2003a).

The Hacker & Abers (2004) rock and mineral database provides compositional details for many common subduction rock types, including 25 MORB-type rocks, 19 hydrated peridotites (10 harzburgites, nine lherzolites) and 21 anhydrated peridotites (10 lherzolites, seven harzburgites, one dunite, wherlite, olivine clinopyroxenite and pyrolite). The percentage of hydrated minerals varies from 0 to 100 vol%. Using an updated version of the Hacker & Abers (2004) worksheet (Hacker, private communication, 2012), we tested for all rock

types allowing an uncertainty range of $\pm 0.1\,\mathrm{km\,s^{-1}}$ in our *Vp* and *Vs*, $\pm 100\,^{\circ}\mathrm{C}$ in *T*, and ± 0.5 GPa in *P*. We did not compare *Vp*/*Vs* ratios, since small variations within the uncertainty constraint of either *Vp* or *Vs*, or both, resulted in substantial misleading differences in the *Vp*/*Vs* values. Hence, we only utilized absolute velocities.

The reliability of our results is quantified by the number of rock solutions per cell (*N*), shown in Fig. 9(b), which in turn depends on the total number of rocks present in our database. For each cell, we calculated the average normalized volume per cent of hydrated minerals contained in the set of rock solutions $\frac{\sum_i^N (\mathrm{Vol})_i}{N}$, where *i* is a rock solution)

We have not used more complete or self-consistent mineral databases, such as Perplex (Connolly 2005) or Theriak (de Capitani & Petrakakis 2010), since these methods generally require that detailed rock and mineral compositions be known. Furthermore, the resolutions associated to our thermomechanical and tomographic data are too limited to justify the use of more complex and precise methods. For the same reason, we think that the use of integrated geophysical–petrological methodologies to model the seismological, density, thermal and compositional variations in the upper mantle (e.g. LitMod3D, Afonso *et al.* 2008, 2010) are pre-mature at this stage in the region under study, as the strength of this approach relies on high-resolution data extending down to ∼400-km depth, while the available data are only seismological. An outcome of thermodynamically self-consistent method is that the *Vp*/*Vs* ratio is not a good indicator of compositional variations in ultramafic mantle rocks in the spinel domain, nor when anelastic attenuation plays an important role (Afonso *et al.* 2008, 2010). On the other hand, these methods yield results compatible with the Hacker & Abers (2004) database in the anharmonic case (at $T \leq 900\,^{\circ}\mathrm{C}$, neglecting viscoelastic relaxation). Since we deal with both crustal and mantle rocks at $T \leq 900\,^{\circ}\mathrm{C}$, we have kept a unified methodology and have included the information from *Vp*/*Vs* ratios in interpretation. An integrated model remains undoubtedly the final aim, and our first-order results represent a first attempt on which to build future more exhaustive models.

Fig. 9(b) shows that the continental and oceanic mantle domains have a large set of rock solutions matching our seismic velocities. The number of rock solutions for the mantle domain is much higher compared to the crustal domain, because it contains fewer compositional varieties (i.e. essentially peridotites); hence, seismic velocities. Nevertheless, our results are considered reliable for both domains, since our seismic velocities in each cell generally fit rocks with similar compositions in major elements (e.g. garnet peridotites) or trends (e.g. hydrated versus dry).

7 DISCUSSION AND INTERPRETATION

7.1 The forearc crust

The forearc crust (domain in burgundy in Fig. 9a) in the flat slab region (<32°S) displays several unusual seismic characteristics which remain difficult to interpret.

Here, the elevated *Vs* and very low *Vp*/*Vs* ratios with respect to the normal slab region, suggest the presence of denser and/or colder rocks, with negligible water content. Indeed, a compositional change around 33°S was suggested by Sallarès & Ranero (2005) and Contreras-Reyes & Osses (2010), who also noted similar results of faster *Vs* ($>4.0\,\mathrm{km\,s^{-1}}$) at 23.5°S than south of 33°S ($Vs < 3.5\,\mathrm{km\,s^{-1}}$), possibly attributed to the higher degree of plutonism and metamorphism in the forearc basement rocks above the flat slab (Ramos *et al.* 1986).

Comparing our seismic velocities with those predicted for typical mafic rocks at these depths using the Hacker & Abers (2004) database, we find that the latter are much faster than our observations, suggesting that the forearc crust above the flat slab is made of either abnormal/deformed mafic rocks or displays prevailing felsic compositions.

We also calculated the seismic velocities at these depths for an average granite composition [74.5 per cent SiO_2, 14 per cent Al_2O_3, 9.5 per cent Na_2O and K_2O, 2 per cent oxides (Fe, Mn, Mg, Ca)] using PerpleX (Connolly 2005) and we obtained much slower seismic velocities ($Vp = 5.9\,\mathrm{km\,s^{-1}}$, $Vs = 2.5\,\mathrm{km\,s^{-1}}$) than our observed values, in particular for *Vs*. Since the Hacker & Abers (2004) rock database does not include other felsic rock compositions to test, we could only examine the relative influence of increasing silica content of any rock, and in this case we observed that *Vp* decreases significantly more than *Vs*. Since our *Vp* is constant throughout the region, we consider that our abnormally high *Vs* in the flat slab region cannot be ascribed to the effects of increased silica content.

Although a compositional change does not fully account for the seismic differences between the northern and southern parts of the forearc crust in this region, it appears to explain better the faster seismic signature of the forearc (Coastal Cordillera) with respect to the main Andean crust further east. Such compositional contrasts are often associated with major shear zones (Twiss & Moore 1992) separating different geomorphotectonic terranes, such as the La Ramada–Aconcagua thrust belt, defining the western Andean front (Principal Cordillera) in the region. This correlation was already reported in northern Chile (15°–23°S) between the forearc and the Altiplano–Puna crusts (Tassara 2005), where a sharp density contrast is associated with high gravity, high resistivity and low *P*-wave attenuation values, and was interpreted as cold and rigid material acting as an indenter into the weaker Altiplano–Puna lithosphere (Tassara *et al.* 2006; Gerbault *et al.* 2009). Ward *et al.* (2013) also image, using ambient noise tomography, sharp shear wave velocity contrasts along geomorphotectonic boundaries in the upper 5 km, exhibiting the Altiplano, the Altiplano–Puna volcanic complex, the Subandes and the Cuyo Basin of the Cuyania terrane as significantly reduced in *Vs*. In our case, the forearc crust in the flat slab region also reflects high gravity anomalies (Tassara, private communication, 2012). However, it lacks any significant seismic attenuation pattern, as shown in Fig. 7a (Deshayes 2008). Nevertheless, a composition or temperature change, reflecting the flat slab region's lower temperature distribution and increased density, should induce simultaneous increases in *Vp* and *Vs*, and not simply in *Vs*, as in our case. In conclusion, normal isotropic mafic rock compositions, higher rock density and lower rock temperatures, do not convincingly explain the shallow (<10-km depth) forearc seismic anomaly.

At greater depths within the forearc, between 35 and 50 km (upper part of the light brown domain in Fig. 9a), an identical seismic anomaly of high *Vs* and very low *Vp*/*Vs* values also occurs at similar latitudes as its shallower counterpart (<32°S), suggesting a relationship between the two.

The deeper forearc anomaly lies within the uncertainty range of the poorly defined seismic Moho (Fromm *et al.* 2004). Hence, it could represent crust or mantle material. Our petrological analysis shows that four mafic rock solutions match the seismic velocities in this depth range and at these *P*–*T* conditions (no. 8 in Fig. 11a shows that no mantle rocks correspond to the observed velocity), whereas mantle rocks explain better the slightly deeper seismic velocities

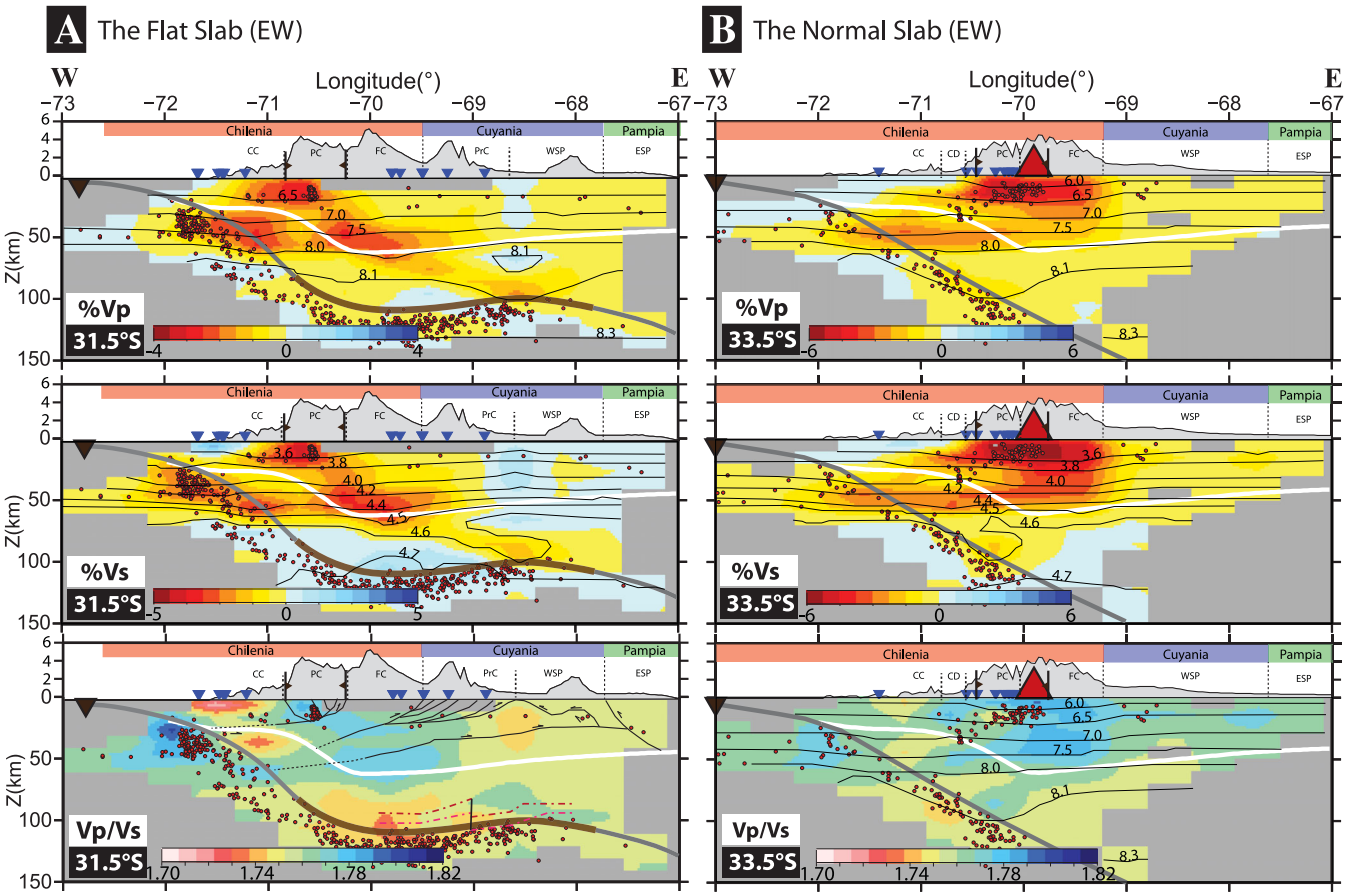

Figure 10. Our seismic tomography results obtained using the slower background velocity model in Fig. 2 (grey line), in comparison to using the faster one (black line, and results shown in Figs 5 and 6) for the (a) flat and (b) normal slab regions. Figure legend as in Fig. 3.

(no. 9 in Fig. 11a). The boundary between the crust and mantle probably lies somewhere in between no. 8 and no. 9 (∼45–50-km depth), a hypothesis supported by the sudden decrease in the slab's seismic activity here (Figs 6a and b) and by a switch to aseismic creep at this depth (50 km, Gardi *et al.* 2006). However, none of the rock compositions obtained from the Hacker & Abers (2004) rock database match the very low *Vp*/*Vs* values observed for the shallow and deep forearc crusts (1.69–1.73) whatever the *P*–*T* conditions considered, underlining their abnormal nature.

A study by Ramachandran & Hyndman (2012) also reported very low *Vp*/*Vs* values (1.65) for the lower forearc crust in the Cascadia subduction zone, between 25 and 35-km depth, equally associated with elevated *Vs* values of 4.1–4.2 km s^{-1}, but with decreased *Vp* (6.6–6.8 km s^{-1}, in contrast with our observation of 7.0–7.1 km s^{-1}. Takei (2002) inferred that adding only 5 per cent silica to a rock decreases significantly its *Vp*/*Vs* ratio. Ramachandran & Hyndman (2012) explained their seismic anomaly with 20 per cent added silica derived from subducted continental material precipitated from upwelling slab fluids. Nevertheless, as mentioned earlier, increasing the silica content of a rock decreases *Vp* substantially more than *Vs*, which is not consistent with our observations.

A link can also be made with the intraslab Punitaqui earthquake aftershock region (1997, *M*w 7.1, 31°S, 70-km depth, Fig. 6b, light green area in Fig. 9a), since it reflects identical seismic behaviours as the two forearc anomalies and it is located directly beneath them in the flat slab region.

In summary, within the flat slab region, two very low *Vp*/*Vs* anomalies occur inside the forearc crust and another inside the slab, for which we can find no reasonable explanation. Simple factors such as normal mafic and ultramafic rock compositions, increased silica concentrations, decreased temperature or increased rock density, are discarded. This leaves the possibility for seismic anisotropy effects as a final explanation, resulting from convergence-induced deformation. MacDougall *et al.* (2012) reported strong seismic anisotropy in the mantle wedge below the forearc and above the flat slab in this region. However, extending this interpretation is beyond the reach of our data.

Finally, we note a link between major faults and regions of high *Vp*/*Vs* ratios in the forearc. For this, we superposed the Farías *et al.*'s (2010) tectonic model of the Andes at 34°S (the La Ramada–Aconcagua thrust belt) onto our seismic tomography (Figs 6 and 10) and attenuation (Fig. 7) models. Extending the faults' paths westwards, a good correlation exists with regions of higher *Vp*/*Vs*, such as the one separating both very low *Vp*/*Vs* anomalies in the forearc crust (at 30-km depth, Fig. 6b) or the one possibly cross-cutting the mantle wedge corner. Thus, we support Farías *et al.* (2010)'s proposition that a crustal shear zone crosses the forearc at mid-crustal depths, extending to the subduction interface and possibly channeling slab fluids into the continental crust, where high *Vp*/*Vs* ratios dominate.

7.2 The main Andean crust

An NS-trending slow velocity and high *Vp*/*Vs* anomaly affects the upper 30 km of the Principal Cordillera crust (red domain in Fig. 9a)

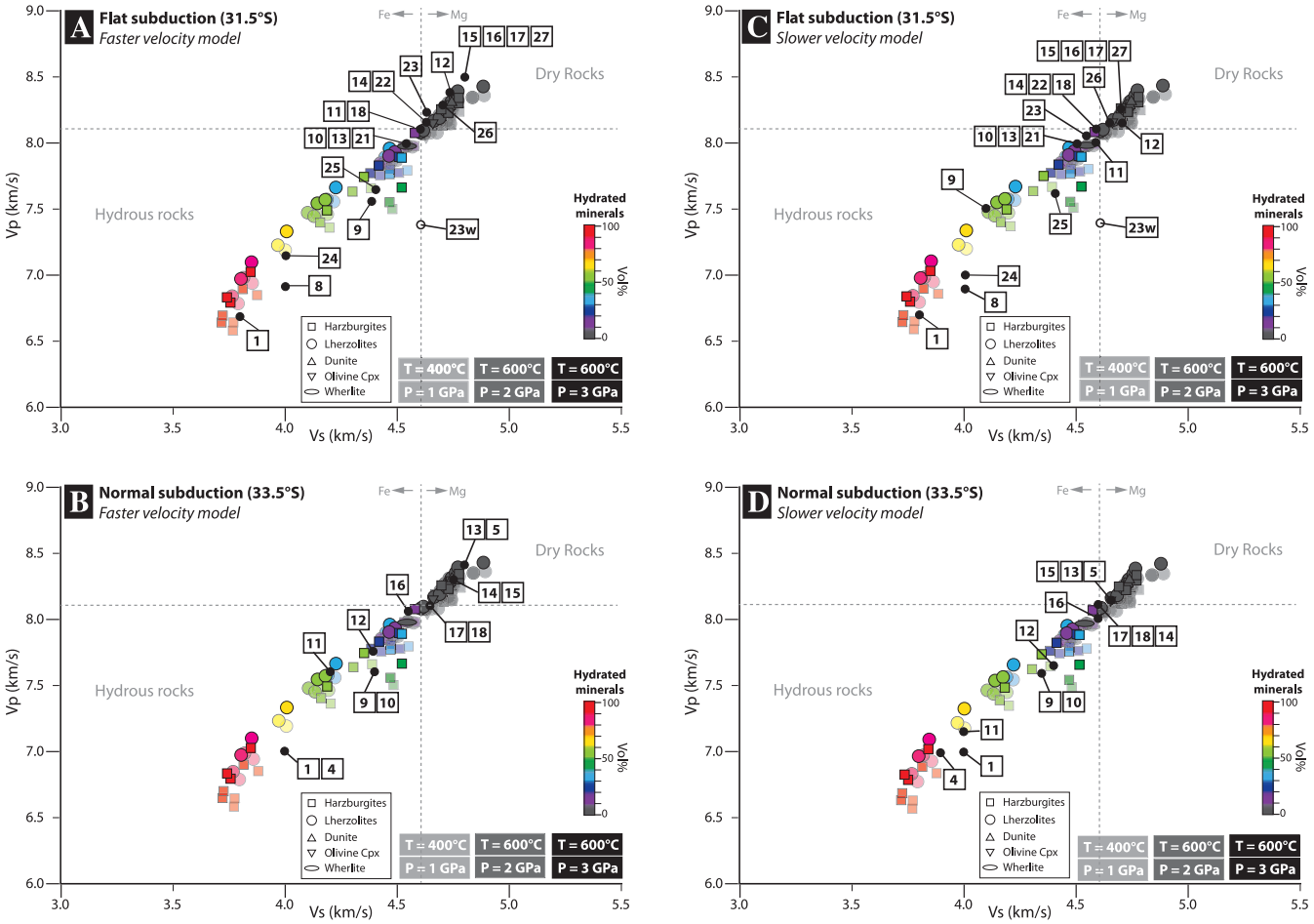

Figure 11. Petrological analyses of two 2-D vertical cross-sections representing the flat (a and c) and normal (b and d) slab regions (31.5°S and 33.5°S, respectively), using the faster (a and b) and slower (c and d) initial velocity models, shown in Fig. 2. Numbers refer to the locations where our seismic velocities were sampled, shown in Fig. 9(a). Predicted seismic velocities (*Vp*, *Vs*) for different ultramafic rocks with varying compositions and percentage of hydrated minerals, representing the continental and oceanic mantles, are calculated at varying pressures (1–3 GPa) and temperatures (400–600 °C) using the Hacker & Abers (2004) worksheet. Increasing the rock's temperature and fluid content decreases its seismic velocities, and increasing its pressure increases its seismic velocities. Rocks with the highest seismic velocities are richer in magnesium (Mg) than iron (Fe). The continental mantle above the flat slab segment is described with an Mg-rich dry composition in the faster initial velocity model, and as borderline between dry and slightly hydrated in the slower velocity model.

and mimics well the location, geometry and dimension of the La Ramada–Aconcagua thrust belt (Figs 1b, 5a, b and 6a, b) (∼100-km wide and ∼20–30-km deep; Ramos *et al.* 2002; Giambiagi *et al.* 2003; Farías *et al.* 2010). Therefore, this slow anomaly is interpreted as the consequence of structural damage, in addition to the regular presence of fluids in fault systems (reflected by the higher *Vp*/*Vs* ratios). In Section 7.1, we interpreted the basement detachment fault of the La Ramada–Aconcagua belt as reaching the subduction interface across the forearc's mid-crust.

The Frontal Cordillera further east, on the other hand, is less affected by such strong velocity reductions, indicating stronger and less fractured crust (Ramos *et al.* 2002), in agreement with its lower seismic activity. The only exception lies in the Cordon del Plata, west of Mendoza city (33°–34°S), displaying similar significant decreases in *Vp* and *Vs* as in the Principal Cordillera, down to 35-km depth (Fig. 5a). Although this region lies outside the limits of the Aconcagua thrust belt, it is also interpreted as structurally damaged (Alvarado *et al.* 2009). In addition, proximity to the active volcanic arc may generate a higher temperature distribution that could explain its slow seismic velocities.

At depth, little is known about the composition and origin of the Andean basement, as there remains little evidence for the existence of the Chilenia terrane, obliterated by abundant intrusions and covered by volcanism and sedimentation. There is no evidence for the location of the Chilenia–Cuyania suture zone at depth (Ramos *et al.* 1986), which would answer the questions about the nature of the Andean basement. However, the continental affinity of the oldest rocks found in the Frontal Cordillera (Caminos *et al.* 1982) supports the existence of Chilenia. Our results show that the lower Andean crust (root) is characterized by significantly reduced seismic velocities with high *Vp*/*Vs* ratios (1.77–1.79) relative to the Andean mid- and Cuyania crusts (Figs 6a and b).

Our seismic velocities, between 50 and 60-km depth, can be explained by jadeite epidote blueschist (74 vol% hydrated minerals corresponding to 3.1 vol% H_2O), garnet granulite and lawsonite amphibole eclogite (57 vol% hydrated minerals corresponding to 3.0 vol% H_2O, 3.35 g cm^{-3}) assemblages. Further down, between 60 and 70-km depth and within the uncertainty range of the seismic Moho (Fromm *et al.* 2004), our seismic velocities match hydrated eclogites (zoisite and zoisite–amphibole eclogites, 32 and 10 vol%

hydrated minerals corresponding to 0.3 and 0.7 vol% H_2O, respectively). However, they could also represent hydrated mantle rocks with an average of 10–30 vol% hydrated minerals (0.8–1.4 vol% H_2O, no. 10, Fig. 11a).

If a slower absolute shear wave velocity was to be considered, as results by Ward *et al.* (2013) suggest, for the petrological analysis of the Andean lower crust, the types of rocks matching these slower velocities would be even further away from an eclogite interpretation, and hence, bring greater support to the hypotheses of a felsic or delaminated lower crust. Using the Hacker & Abers (2012 version) worksheet, we have simulated the seismic velocities for MORB-type rocks at depths between ∼50 and 60-km depth (the Andean root) and compared them with seismic velocities 5 per cent slower than our values, considering an uncertainty range of 0.1 km s^{-1} for seismic velocities, 0.5 GPa for pressure and 100 °C for temperature, as described in Section 6. The results indicate that, at these slower seismic velocities, no eclogite occurs below $Vp = 7.5$ km s^{-1} and $Vs = 4.3$ km s^{-1}, and the majority of mafic rock solutions are hydrated, containing between 53 per cent and 87 vol% hydrated minerals. Therefore, our petrological interpretation would remain unchanged, and our conclusions are that the Andean lower crust is most likely hydrated, probably non-eclogitized or only partially eclogitized below 60-km depth, and either mafic or felsic. Gilbert *et al.* (2006) also reported the absence of eclogitization in the deepest portions of the Main Andean crust.

The absence of significant eclogitized crustal root can be explained by the following: (1) the rock composition is too felsic to transform into eclogite. This is highly likely, since felsic rocks have slower seismic velocities than mafic rocks and the Andean crust is suspected to encompass the continental Chilenia terrane; (2) the lower crust temperature is too low for eclogite transformation to occur efficiently, even in the presence of catalyzing fluids (Artemieva & Meissner 2012) and (3) crustal delamination occurring prior to horizontal subduction may have removed the previously denser eclogitic lower crust, by a mechanism of gravitational instability (DeCelles *et al.* 2009). Crustal delamination was proposed by Kay & Gordillo (1994) to explain the deep and old crustal signatures in the Pocho lava rocks above the resubducting slab further east (65°W, 32°S). Therefore, the Andean lower crust's low velocities can be explained by a felsic or a mafic non-eclogitized crustal root, with the presence of fluids. Such a felsic root would attest for the presence of Chilenia and provide insight on the location of the Chilenia–Cuyania suture zone at depth.

7.3 The backarc crust

A careful interpretation of our backarc seismic velocities is required, as our checkerboard test shows leakage from less well-resolved cells into the backarc region, though the latter is locally well resolved in our spike test.

The Grenvillian Cuyania terrane (Precordillera and western Sierra Pampeanas, purple domain in Fig. 9a) stands out as a fast *Vp* and *Vs* anomaly down to 80-km depth, in agreement with Porter *et al.* (2012) using ambient noise tomography, with moderately low *Vp*/*Vs* ratios (1.70–1.74) (Fig. 6d). Consistent with these observations, Cuyania is also mapped as a high gravity anomaly, overprinted by a low-temperature distribution until 37°S (Tassara *et al.* 2006). These observations reflect its mafic/ultramafic and cold and old character (Ramos *et al.* 1986, 2002; Ramos 2004). However, we can only observe its high *Vp* until ∼33°S and high *Vs* until ∼32°–32.5°S, rather than 37°S (Figs 5a and 6d). The largest anomaly is situated more-or-less beneath San Juan city, which is directly above the inferred subducting JFR track.

Multiple seismic and gravity studies estimated a crustal thickness of 60 km beneath the Precordillera and 50–55 km beneath the western Sierra Pampeanas (Regnier *et al.* 1994; Fromm *et al.* 2004; Alvarado *et al.* 2005, 2007, 2009; Calkins *et al.* 2006; Gilbert *et al.* 2006; Corona 2007; Castro de Machuca *et al.* 2012). All interpretations involve the existence of a dense eclogitized lower crust to explain seismic velocity jumps in the crust and their unexpected high gravity values relative to their average low elevations (∼2 and 1 km, respectively) (Miranda 2001; Alvarado *et al.* 2005, 2007; Gilbert *et al.* 2006). Indeed, our high seismic velocities for Cuyania (around 68.75°W) confirm the presence of eclogites (amphibole and zoisite eclogites, with 26 and 10 vol% hydrated minerals, corresponding to 0.6 and 0.3 vol% H20, respectively, 3.50 g cm^{-3}) below 50 km depth, and occurring 10 km shallower than in the Andean crustal root (Section 7). At shallower depths, between 40 and 50-km depth, lawsonite amphibole eclogite (57 vol% hydrated minerals, corresponding to 3 vol% H_2O, 3.35 g cm^{-3}) could occur, as well as jadeite epidote blueschist (74 vol% hydrated minerals corresponding to 3.1 vol% H_2O) and garnet granulite assemblages. Since eclogite is not seismically distinguishable from mantle rocks, we are unable to provide information about the maximum depth extent of this eclogitic layer. However, it can comprise at least the lower 10 km of the Cuyania crust (50–60 km) and possibly shallower levels (40–50 km). The presence of eclogite supports a mafic composition, indicating that Cuyania (and not Chilenia) forms the backarc basement, constraining further the suture zone location between these terranes.

7.4 The continental mantle: forearc and arc domains

Whether the flat slab retains or releases fluids is a key information to better constrain the reasons for its flat geometry and the fate of deformation in the overriding lithosphere, since fluids decrease the bulk rock density, increase buoyancy and reduce rock strength (e.g. Reynard 2013). In the following, we describe our interpretation of the continental mantle properties (light brown domain in Fig. 9a) successively from the westernmost forearc, through the main arc, to the easternmost backarc domain.

The seismic velocities in the forearc mantle above the flat and normal slabs and in between 50 and 60-km depth, match at ∼70 per cent with serpentinized mantle rocks (six of nine, and five of seven rock types for cells referred as no. 9 and no. 10, respectively, Fig. 11a), and comprise an average of 30 vol% hydrated minerals: amphibole (avg. 15 vol%), talc (avg. < 5 vol%), chlorite and Å-phase (avg. <10 vol%). This is in agreement with the locally higher *Vp*/*Vs* ratios observed in the mantle in this depth range (Figs 6a and b). Down to 80-km depth, the forearc mantle exhibits a pronounced low *P*-wave attenuation anomaly (Figs 7a and b, Deshayes 2008). However, the effects on seismic attenuation of saturated versus undersaturated fluid conditions are complex and difficult to assess (Toksöz *et al.* 1979).

The small variations (∼0.05 km s^{-1}) in the seismic velocities of the forearc and arc mantle domains, above both normal and flat slabs (Figs 11a and b), imply similar degrees of mantle hydration; yet, the mantle above the normal slab strongly attenuates *P* and *S* waves (Fig. 7c; Deshayes 2008) and appears able to produce sufficient partial melts to feed the overlying volcanoes. Hence, we question the role of mantle temperature in causing similar degrees of slab dehydration above the flat and normal slabs, and in triggering the

mantle wedge's partial melting above the normal slab only. Possibly, the mantle wedge adjacent to the normal slab is unusually cold and dry compared to usual subduction circumstances, or alternatively the mantle above the flat slab is unexpectedly hydrated given its lower temperature distribution.

Directly south, above the normal slab region (33.5°–35°S), the erupted lavas from the first three volcanoes (Tupungatito, San José and Maipo) reflect the return to a normal subduction angle at depth and describe higher degrees of fractionation and crustal contamination than the rest of the Southern Volcanic Zone (SVZ). This is due to longer magma ascent and residence times in the crust (Michael Dungan, private communication, 2012). It can be explained by (1) smaller magma production relative to the rest of the SVZ, reflecting poor slab dehydration processes or low mantle temperatures, or by (2) high crustal compressional stresses associated to the flat slab, impeding magma ascent. In both cases, the flat slab conditions to the north appear to affect the normal slab region directly to its south over a few hundred kilometres, at least between ∼32.5° and 34.5°S. Based on geological evidence, Folguera & Ramos (2011) proposed that the current Pampean flat slab once extended further south until 38°S at 12 Ma, before its southern segment progressively steepened to its present angle of subduction (∼30°) at 5 Ma. This hypothesis might explain the similar seismic structure of the mantle wedges above both normal and flat slabs in the region, and also renders our assumed 'normal' subduction conditions at 33.5°S closer to a transitional state than with more normal conditions found further south (>38°S). Therefore, although the tectonics near the surface change rapidly as a response to the dramatic shift in the slab geometry at depth, the continental mantle at depth appears less abruptly affected (seismically speaking) by these sudden changes; perhaps owing to relatively homogeneous viscous behaviour.

7.5 The continental mantle: backarc domain

The continental mantle above the main flat slab domain, from about 71°W to 69°W and deeper than 70 km, is fast in *Vp* and *Vs*, with *Vp*/*Vs* ratios mainly around 1.75–1.77 (Fig. 6b), in agreement with previous interpretations of a cold and dry mantle (no. 12, 14, 22 and 23 in Figs 9a and 11a). Furthermore, we find that mostly Opx- and Mg-rich garnet peridotites (lherzolites and harzburgites) match these high seismic velocities, a conclusion also reached by Wagner *et al.* (2005, 2006, 2008) based on another processing method of the CHARGE seismic data. Afonso *et al.* (2010) demonstrated that *Vp*, and particularly *Vs*, are sensitive to the Mg# (Mg/[Mg-Fe]) of peridotites at such depths, which is high in our case; an indication that the continental mantle above the flat slab is likely depleted. Subduction-related volcanism, followed by the absence of a warm asthenospheric corner wedge for several million years, logically explains this depleted signature and high Mg#.

The uppermost continental mantle immediately below the Frontal Cordillera crust (no. 13 in Figs 9a and 11a) displays significant locally attenuated *P* waves (Fig. 7a; Deshayes 2008) and slower seismic velocities relative to the surrounding mantle. These velocities match partially hydrated mantle rocks (avg. 10–20 vol% hydrated minerals, corresponding to 0.8–1.4 vol% H_2O) and are similar to those recorded further east near the Moho, directly beneath the Cuyania crust (no. 21 in Figs 9a and 11a). However, the proximity of this material to the ill-defined Moho could indicate that it represents crust material instead (hydrated eclogites, see Section 7). One way of determining whether the seismic variations observed in the continental mantle are affected by temperature or composition is to calculate the ratio between density and shear wave velocity (ρ/*Vs*) for each cell of the model, a technique proposed by Afonso *et al.* (2010) as the most robust indicator for a compositional change, provided that self-consistently determined density, shear wave and seismic attenuation data be available. This may be the target of future work.

Further to the east, in between 68°W and 69°W and at 95-km depth, the mantle directly above the flat slab's eastern extremity displays significant reductions in *Vp* and *Vs* and increased *Vp*/*Vs* ratios over a small volume of 100 × 100 × 20 km^3 (Figs 5c and 6a, b, d, location no. 23 in Fig. 9a). This observation is consistent with other geophysical investigations which highlighted this region as strongly reduced in *Vp* (Wagner *et al.* 2005; Bianchi *et al.* 2013) and in *Vs* (4.0 km s^{-1} according to Porter *et al.* 2012), highly attenuated in *S* waves (Fig. 7a, Deshayes 2008), and significantly conductive (Booker *et al.* 2004; Orozco *et al.* 2013). All indicate fluids effects. The geographical position of this anomaly (no. 23) coincides with the subducting JFR track (Figs 5c and 6a, b, d), indicating that the oceanic lithosphere along the seamount ridge may dehydrate and release fluids into the overlying continental mantle in this area. On the other hand, although Wagner *et al.* (2005) also found strong *Vp* reductions associated to this area, nonetheless their *Vs* remains high and results in very low *Vp*/*Vs* values (∼1.65). In comparison, our model indicates a similar *Vs* value, but much higher *Vp* and *Vp*/*Vs* ratio (Fig. 6d). By analysing mantle rock seismic properties over a wide range of *P*–*T* conditions appropriate for this area, we did not find any correspondence in Hacker & Abers's (2004) database with Wagner *et al.*'s (2005) seismic velocities (no. 23w in Fig. 11a), suggesting that their *Vp* might be too low because of their use of a global background model. Using a global model such as IASPEI-91 does not lead to consistent interpretations (no. 23w, Figs 11a and c); this model is however too far from the local structure to make a comparison worthwhile. Interpreting our own absolute seismic velocities for this anomaly allows a fit only with dry garnet peridotites listed in Hacker & Abers (no. 23 in Fig. 11a), contradicting hydrated mantle conditions reflected by our seismic velocity perturbation at this location.

To remedy this paradox of fast seismic velocities where dehydration is expected above the eastern tip of the flat slab (Booker *et al.* 2004; Porter *et al.* 2012; Bianchi *et al.* 2013; Orozco *et al.* 2013), we tested our results when using a ∼3.0–3.5 per cent slower background 1-D velocity model for mantle depths (Fig. 2, grey line). This model is the slowest at mantle depths which comprises the spectrum of reasonable 1-D model possibilities that fit best our data, and it is equivalent to those used by Sanchez *et al.* (2013) for western Argentina and by Haberland *et al.* (2006) for the central Chilean Maule region. Our results are shown in Figs 10(a) and (b) for the flat (31.5°S) and normal (33.5°S) slab regions. This model produces a slightly higher traveltime misfit for earthquake localization compared to our first model used (see Section 3). The effects on the continental mantle above the eastern tip of the flat slab, between 90 and 100-km depth, are a reduction in *Vp* and *Vs* of the order of 0.2 and 0.1 km s^{-1}, respectively, now showing a *Vp* of 8.0–8.1 km s^{-1} and *Vs* of 4.5–4.6 km s^{-1} (no. 23 in Figs 10a and 11c) which fit mostly dry rocks and slightly serpentinized peridotites (Fig. 11c), with an average of 7 vol% hydrated minerals in total.

These results show that the initial velocity model influences the final velocity results. However, our petrological interpretation, based on our absolute values, remains consistent with a mainly dry continental mantle composition; whereas, some localized mantle hydration is suggested by both our observed seismic perturbation and

other methods of investigations. A hypothesis explaining this paradox would be that fluids stored here and their small quantity are less detectable by seismic methods rather than electrical resistivity surveys for instance (Unsworth & Rondenay 2013); hence our seismic velocities are not reduced enough to match the properties of hydrated rocks.

To resume, in accounting for inhomogeneous seismic properties in the continental mantle, we agree with previous studies that hypothesize the flat slab portion may dehydrate along the JFR track prior to its resubduction into the deeper mantle, due to its proximity to the hot asthenosphere directly to the east. We expect those released fluids to be stored in the adjacent continental mantle, where slower seismic velocities can be observed (no. 23, Fig. 11). We also suggest the possibly for these fluids to migrate upwards into the Andean lower crust via crustal shear zones that cross-cut the mantle, as suggested by the locally higher *Vp*/*Vs* ratios and the seismic attenuation below the Frontal Cordillera crust. Crustal faults are believed to penetrate into the continental mantle (e.g. Fromm *et al.* 2004; Gilbert *et al.* 2006), given the region's low temperature distribution and, thus intensive shearing may occur throughout the plate interface and continental mantle. Note that the low *Vp* and *Vs* anomalies (Figs 6a and 10a) span the entire width of the continental lithosphere along a $\sim 30^{\circ}$ inclined zone which links the forearc foothills down to the eastern tip of the flat slab. This domain may represent a damaged zone which may act as a weak zone in the future evolution of the subduction zone geometry.

7.6 The oceanic lithosphere

If we consider a normal oceanic crustal thickness of less than 10 km, as observed offshore (∼8-km thick along the JFR; Kopp *et al.* 2004), then the vertical resolution of our model (10 km) limits us to studying only its oceanic mantle.

The oceanic lithosphere in the flat slab region, down to about 60–70-km depth, is characterized by low seismic velocities and high *Vp*/*Vs* ratios (1.80, Figs 6a and b). At 25-km depth, these velocities match with fully serpentinized mantle rocks (no. 1, 100 vol% hydrated minerals) and with 60–70 vol% (no. 24), 50–60 vol% (no. 25) and 0–20 vol% serpentinization at 40, 50 and 70-km depths, respectively (Fig. 11a), indicating a slowly dehydrating slab with depth. Similar results are obtained for the normal slab region, whereby the slab appears to be 50–60 vol% serpentinized at 50-km depth (no. 9–10), and hardly hydrated (no. 17–18) or totally dry (no. 14–13) below 70-km depth (Fig. 11b). Although our ray coverage is to be poor above 50-km depth in the normal intraslab region, extrapolated seismic velocities tend to be consistent with highly serpentinized rocks. Furthermore, the plate interface at 25-km depth in the flat slab region is likely a zone of strong fluid concentration (no. 1 in Fig. 11a), shown by the very high *Vp*/*Vs* ratios and decreased *Vs* (Figs 6a and b), probably related to the effects of fluid-filled pore compaction and primary rock dehydration reactions, causing expulsion of slab fluids at these depths (Kirby *et al.* 1996; Peacock 2001; Hacker *et al.* 2003a).

Although the slight velocity variations ($\sim 0.05\ \mathrm{km\,s^{-1}}$) observed between the normal and flat slab regions show no difference in predicted rock compositions, they nevertheless cause non-negligible variations in the *Vp*/*Vs* ratios. The higher *Vp*/*Vs* ratios above 60–70-km depth in the flat slab region suggest higher plate hydration along the subducting JFR. Indeed, there might be intense lithospheric hydration offshore, according to seismic and gravity investigations over the ∼500-km wide Challenger Fracture zone, which the JFR is part of (Yáñez *et al.* 2002; Grevemeyer *et al.* 2003, 2005; Kopp *et al.* 2004; Ranero *et al.* 2005; Clouard *et al.* 2007; Contreras-Reyes & Osses 2010), and where intense fracturing and faulting allow particularly deep sea water penetration to occur, at least down to 20-km depth (Ranero *et al.* 2005; Clouard *et al.* 2007).

Along the flat slab segment, Gans *et al.* (2011) used receiver function analyses to measure a probable thicker oceanic crust (∼15 km compared to ∼8 km, Kopp *et al.* 2004) spanning a wider area (∼300 km N–S) than the widths of the JFR measured offshore and the dense flat slab's seismicity band (both 100-km wide; white line and band in Figs 1 and 5; Kopp *et al.* 2004). They also interpreted a vertical offset along an inherited fault at similar depths (∼69°W, dotted red/pink lines shown in Figs 6a, b, 7a and 10a). Non- or partially eclogitized oceanic crust is invoked as the main factor inducing flat subduction in this region (Martinod *et al.* 2005, 2010; Gans *et al.* 2011), with basaltic crust being about $0.5\ \mathrm{g\,cm^{-3}}$ lighter than 'mature' eclogite ($3.5\ \mathrm{g\,cm^{-3}}$). The conjoint effect of an overthickened and non-eclogitized oceanic crust on slab buoyancy would be furthermore enhanced.

Our maximum vertical resolution of 10 km should enable us to detect a 15-km-thick oceanic crust. In the case of an overthickened non-eclogitized oceanic crust, a slow velocity anomaly should appear. Considering flat slab *P*–*T* conditions (400–800 °C at 2–4 GPa; Van Hunen *et al.* 2002), normal average basaltic crust has *Vp* values between 7.2 and $7.6\ \mathrm{km\,s^{-1}}$ (Hacker *et al.* 2003a). Not only do our results and those of Porter *et al.* (2012) (showing a flat slab segment with $Vs = 4.9\ \mathrm{km\,s^{-1}}$) contradict Gans *et al.* (2011)'s observation of a non-eclogitized thick crust, but our fast seismic velocities are only compatible with very dense and dry eclogites ($3.5–3.6\ \mathrm{g\,cm^{-3}}$), arguing against the concept of slab buoyancy. Therefore, it is unlikely that our seismic velocities here reflect an overthickened oceanic crust.

Testing our results using a slower background model at flat slab depths (Fig. 2, grey line), the resulting lower seismic velocities (*Vp* $\sim 8.2\ \mathrm{km\,s^{-1}}$, *Vs* $\sim 4.7\ \mathrm{km\,s^{-1}}$, Fig. 10a) in the upper 20 km of the flat slab now match zoisite and amphibole eclogites (10 per cent and 26 vol% hydrated minerals, corresponding to 0.3 and 0.6 vol% H_2O, respectively, average $3.55\ \mathrm{g\,cm^{-3}}$), nevertheless, their predicted densities are equivalently high, with an excess of $0.2–0.3\ \mathrm{g\,cm^{-3}}$ relative to normal mantle ($3.3\ \mathrm{g\,cm^{-3}}$); and so the paradox of a buoyant slab persists.

Considering an oceanic crust of less than 10 km in thickness (our vertical minimum resolution), then our seismic velocities, using both background models, represent oceanic mantle with corresponding rock types that still predict dry and dense ($3.4\ \mathrm{g\,cm^{-3}}$) peridotites (no. 15–17, 27 in Figs 9a and 11a, c). It is important to note that our petrological interpretation remains consistent despite the changes induced by varying the initial 1-D model.

To summarize, the flat slab portion is most likely composed of dry oceanic mantle, regardless of which background model we used, with an oceanic crust of normal thickness (<10 km), non- or partially eclogitized, but nonetheless dense ($3.56\ \mathrm{g\,cm^{-3}}$). This interpretation agrees with the following evidences supporting the notion of fluid storage in the slab and progressive fluid release into the overlying mantle during its descent into the deep mantle:

(1) The concentration of flat slab seismicity along the JFR track (Fig. 1c) caused by undergoing eclogitization phase transformations in the oceanic crust (e.g. Kirby *et al.* 1996; Hacker *et al.* 2003b),

(2) The flat slab buoyancy (however probably does not explain the full extent of this feature in this region),

(3) The high mantle conductivity values adjacent to the resubducting slab down to >300-km depth (Booker *et al.* 2004),

(4) The recent volcanism in San Luis located in the Sierras Cordoba province (65°W dated at 1.9 Ma; Kay & Abbruzzi 1996).

8 CONCLUSIONS AND PERSPECTIVES

In conclusion, our results show that there are significant seismic differences between the flat and normal slab regions of central Chile and western Argentina:

(1) The forearc crust above the flat slab (<32°S) exhibits high *Vs* and very low *Vp*/*Vs* ratios in two distinct depth ranges, 0–10 and 35–50 km. No normal rock type was found to correlate with these seismic velocities. However, we suggest possible links with transient short timescale variations of the Punitaqui aftershock area, the flat slab geometry and/or seismic anisotropy.

(2) We interpret localized regions of higher *Vp*/*Vs* ratios in the forearc crust and mantle wedge as hydrated zones representing basement detachment shear zones reaching the subduction interface and channeling slab-derived fluids into the Andean crust.

(3) The Andean crust throughout the region is characterized by significantly reduced seismic velocities and relatively high *Vp*/*Vs* ratios, especially in the depth ranges of 0–30 and 40–70 km. The shallow anomaly is explained by intense structural damage correlated with the La Ramada–Aconcagua thrust belt (consistent with surface wave and ambient noise tomography studies by Porter *et al.* 2012 and Ward *et al.* 2013). The deeper Main Andean crustal root anomaly is interpreted as a fluid-bearing and either mafic non-eclogitized or felsic crust, coinciding with the deep extent of the Chilenia terrane.

(4) The backarc crust exhibits fast seismic velocities and low *Vp*/*Vs* ratios, outlining the Cuyania terrane, which are compatible with eclogitic compositions below 50-km depth, supporting many previous interpretations (e.g. Gilbert *et al.* 2006; Alvarado *et al.* 2007). However, our spatial resolution of this area is limited.

(5) Little seismic variation is observed in the mantle wedges above 70-km depth, both in the flat and normal slab regions, describing similar levels and depths of hydration. This similarity is consistent with recent reconstructions of past flat subduction in south central Chile (Folguera & Ramos 2011).

(6) The continental mantle in the flat slab region is generally characterized by fast seismic velocities and relatively low *Vp*/*Vs* ratios, probably enhanced by the region's low temperature distribution, and matching dry Opx- and Mg-rich peridotites at such depths, as previously suggested (e.g. Wagner *et al.* 2005, 2006). This coincides well with the intense deformation style and the cessation of arc volcanism at the surface.

(7) We show evidence that the subducting oceanic crust along the JFR track locally dehydrates at the eastern tip of the flat slab (68.5°W/31.5°S) before resubduction occurs, suggesting that fluids are retained within the flat slab and some are stored in the continental mantle above it, as supported by numerous other studies (e.g. Booker *et al.* 2004; Wagner *et al.* 2006, 2008; Bianchi *et al.* 2013; Orozco *et al.* 2013).

(8) Contrary to Gans *et al.* (2011), we interpret the oceanic crust along the flat slab segment as thinner than our model's vertical resolution of 10 km and non- or only partially eclogitized. This hypothesis is consistent with (i) our interpretation of ongoing dehydration along the JFR, (ii) the concentration of seismic activity along the flat slab segment and (iii) the higher mantle conductivity values (Booker *et al.* 2004) and recent volcanism further east (Kay & Gordillo 1994). Nevertheless, the high rock densities predicted for the flat slab segment constitute a paradox to the flat slab buoyancy, which we do not manage to explain.

Our seismic data therefore does not support the presence of buoyant material in the flat slab area, and therefore other interpretations need to be considered. Analogue and numerical subduction models are still being actively developed to better assess the causes for flat subduction, not only testing for the subducting ridge buoyancy and overriding plate motion (e.g. Van Hunen *et al.* 2004; Martinod *et al.* 2010, 2013), but also for heterogeneities in the continental lithospheric thickness (O'Driscoll *et al.* 2012), strength variations in both oceanic and continental lithospheres (Gerbault *et al.* 2009), phase transitions in the orogenic crust (e.g. DeCelles *et al.* 2009) and slab folding over the 660-km depth discontinuity zone (Gibert *et al.* 2012; Cerpa *et al.* 2014).

Determining the fate of the subducted oceanic crust remains crucial for assessing the gravitational contribution to driving forces involved in the central Chilean flat subduction zone, as well as for quantifying dehydration processes in subduction zones in general.

ACKNOWLEDGEMENTS

Local data were obtained thanks to projects FONDECYT 1020972-1050758, and IRD- GéoAzur campaigns. MM and GN are supported by the GlobalSeis project (ERC 226837). GR's participation in this project is supported by an NSERC grant (Natural Sciences and Engineering Research Council of Canada) and by Carleton University. We are very grateful to all those who have actively discussed and debated this work with us, providing us new insights and challenges, including Andrès Tassara, Lara Wagner, Eric Ferre, Stephan Rondenay and Manuele Faccenda. We also would like to thank Perrine Deshayes, who shared with us her seismic attenuation tomography results for this region, and two anonymous reviewers whose comments were very useful in revising the paper.

REFERENCES

Afonso, J.C., Fernández, M., Ranalli, G., Griffin, W.L. & Connolly, J.A.D., 2008. Integrated geophysical-petrological modeling of the lithosphere and sublithospheric upper mantle: methodology and applications, *Geochem. Geophys. Geosyst.,* **9**(5), doi:10.1029/2007GC001834.

Afonso, J.C., Ranalli, G., Fernàndez, M., Griffin, W.L., O'Reilly, S.Y. & Faul, U., 2010. On the Vp/Vs–Mg# correlation in mantle peridotites: implications for the identification of thermal and compositional anomalies in the upper mantle, *Earth planet. Sci. Lett.,* **289**(3), 606–618.

Allmendinger, R.W., Jordan, T.E., Kay, S.M. & Isacks, B.L., 1997. The evolution of the Altiplano-Puna plateau of the Central Andes, *Annu. Rev. Earth planet. Sci.,* **25**(1), 139–174.

Alvarado, P. & Ramos, V.A., 2011. Earthquake deformation in the northwestern Sierras Pampeanas of Argentina based on seismic waveform modeling, *J. Geodyn.,* **51**(4), 205–218.

Alvarado, P., Beck, S., Zandt, G., Araujo, M. & Triep, E., 2005. Crustal deformation in the south-central Andes backarc terranes as viewed from regional broad-band seismic waveform modeling, *Geophys. J. Int.,* **163**(2), 580–598.

Alvarado, P., Beck, S. & Zandt, G., 2007. Crustal structure of the south-central Andes Cordillera and backarc region from regional waveform modeling, *Geophys. J. Int.,* **170**(2), 858–875.

Alvarado, P., Pardo, M., Gilbert, H., Miranda, S., Anderson, M., Saez, M. & Beck, S., 2009. Flat-slab subduction and crustal models for the seismically active Sierras Pampeanas region of Argentina, in *Backbone of the Americas: Shallow Subduction, Plateau Uplift, and Ridge and Terrane*

Collision, Geol. Soc. Am. Memoirs, No. 204, pp. 261–278, Geological Society of America.

Anderson, M., Alvarado, P., Zandt, G. & Beck, S., 2007. Geometry and brittle deformation of the subducting Nazca Plate, Central Chile and Argentina, *Geophys. J. Int.,* **171**(1), 419–434.

Araujo, M. & Suarez, G., 1994. Geometry and state of stress of the subducted Nazca Plate beneath central Chile and Argentina: evidence from teleseismic data, *Geophys. J. Int.,* **116,** 283–303.

Artemieva, I.M. & Meissner, R., 2012. Crustal thickness controlled by plate tectonics: a review of crust-mantle interaction processes illustrated by European examples, *Tectonophysics,* **530,** 18–49.

Barazangi, M. & Isacks, B.L., 1976. Spatial distribution of earthquakes and subduction of the Nazca plate beneath South America, *Geology,* **4**(11), 686–692.

Barrientos, S., Vera, E., Alvarado, P. & Monfret, T., 2004. Crustal seismicity in Central Chile, *J. South Am. Earth Sci.,* **16,** 759–768.

Bianchi, M. *et al.*, 2013. Teleseismic tomography of the southern Puna plateau in Argentina and adjacent regions, *Tectonophysics,* **586,** 65–83.

Booker, J.R., Favetto, A. & Pomposiello, M.C., 2004. Low electrical resistivity associated with plunging of the Nazca flat slab beneath Argentina, *Nature,* **429**(6990), 399–403.

Cahill, T. & Isacks, B.L., 1992. Seismicity and shape of the subducted Nazca plate, *J. geophys. Res.,* **97**(B12), 17 503—17 529.

Calkins, J.A., Zandt, G., Gilbert, H.J. & Beck, S.L., 2006. Crustal images from San Juan, Argentina, obtained using high frequency local event receiver functions, *Geophys. Res. Lett.,* **33**(7), doi:10.1029/2005GL025516.

Caminos, R., Cingolani, C.A., Hervé, F. & Linares, E., 1982. Geochronology of the pre-Andean metamorphism and magmatism in the Andean Cordillera between latitudes 30 and 36 S, *Earth Sci. Rev.,* **18**(3), 333–352.

Castro de Machuca, B., Perarnau, M., Alvarado, P., López, G. & Saez, M., 2012. Modelo cortical sismológico y petrológico para el sudoeste de la sierra de Pie de Palo, provincia de San Juan, *Rev. Asoc. geol. Argent.,* **69**(2), 179–186.

Cerpa, N.G., Hassani, R., Gerbault, M. & Prévost, J.H., 2014. A fictitious domain method for lithosphere/asthenosphere interaction: application to periodic slab folding in the upper mantle, *Geochem. Geophys. Geosyst.,* **15**(5), 1852–1877.

Clouard, V., Campos, J., Lemoine, A., Perez, A. & Kausel, E., 2007. Outer rise stress changes related to the subduction of the Juan Fernandez Ridge, central Chile, *J. geophys. Res.,* **112**(B5), doi:10.1029/2005JB003999.

Connolly, J.A.D., 2005. Computation of phase equilibria by linear programming: a tool for geodynamic modeling and its application to subduction zone decarbonation, *Earth planet. Sci. Lett.,* **236**(1), 524–541.

Contreras-Reyes, E. & Osses, A., 2010. Lithospheric flexure modelling seaward of the Chile trench: implications for oceanic plate weakening in the Trench Outer Rise region, *Geophys. J. Int.,* **182**(1), 97–112.

Corona, G., 2007. Estructura Litosférica del Sistema Andes Sierras Pampeanas en la Banda 30°S–31°S a Partir de Datos de Gravedad y Sísmicos, *Undergraduate final work thesis*, San Juan, Argentina, Facultad de Ciencias (in Spanish).

Cundall, P.A. & Board, M., 1988. A microcomputer program for modeling large strain plasticity problems, in *Proceedings of 6th International Conference on Numerical Methods in Geomechanics,* Innsbruck, Austria.

de Capitani, C. & Petrakakis, K., 2010. The computation of equilibrium assemblage diagrams with the Theriak/Domino software, *Am. Mineral.,* **95**(7), 1006–1016.

DeCelles, P.G., 2004. Late Jurassic to Eocene evolution of the Cordilleran thrust belt and foreland basin system, western USA, *Am. J. Sci.,* **304**(2), 105–168.

DeCelles, P.G., Ducea, M.N., Kapp, P. & Zandt, G., 2009. Cyclicity in Cordilleran orogenic systems, *Nature Geosci.,* **2**(4), 251–257.

Deshayes, P., 2008. Tomographie en vitesse et en atténuation de la zone de subduction au Chili central-ouest de l'Argentine (29°S–34°S) à partir de données sismologiques locales: apport à l'étude de la composition minéralogique, *Doctoral dissertation,* Université de Nice Sophia-Antipolis (in French).

Espurt, N., Funiciello, F., Martinod, J., Guillaume, B., Regard, V., Faccenna, C. & Brusset, S., 2008. Flat subduction dynamics and deformation of the South American plate: insights from analog modeling, *Tectonics,* **27**(3), TC3011, doi:10.1029/2007TC002175.

Farías, M., Comte, D., Charrier, R., Martinod, J., Tassara, A. & Fock, A., 2010. Crustal-scale structural architecture of the Central Chile Andes based on 3D seismic tomography, seismicity, and surface geology: implications for mountain building in subduction zones, *Tectonics,* **29,** doi:10.1029/2009TC002480.

Folguera, A. & Ramos, V.A., 2011. Repeated eastward shifts of arc magmatism in the Southern Andes: a revision to the long-term pattern of Andean uplift and magmatism, *J. South Am. Earth Sci.,* **32**(4), 531–546.

Fromm, R., Zandt, G. & Beck, S.L., 2004. Crustal thickness beneath the Andes and Sierras Pampeanas at 30 S inferred from Pn apparent phase velocities, *Geophys. Res. Lett.,* **31**(6), doi:10.1029/2003GL019231.

Gans, C.R., Beck, S.L., Zandt, G., Gilbert, H., Alvarado, P., Anderson, M. & Linkimer, L., 2011. Continental and oceanic crustal structure of the Pampean flat slab region, western Argentina, using receiver function analysis: new high-resolution results, *Geophys. J. Int.,* **186**(1), 45–58.

Gardi, A., Lemoine, A., Madariaga, R. & Campos, J., 2006. Modeling of stress transfer in the Coquimbo region of central Chile, *J. geophys. Res.,* **111**(B4), doi:10.1029/2004JB003440.

Gerbault, M., Cembrano, J., Mpodozis, C., Farias, M. & Pardo, M., 2009. Continental margin deformation along the Andean subduction zone: thermo-mechanical models, *Phys. Earth planet. Inter.,* **177**(3), 180–205.

Giambiagi, L.B. & Ramos, V.A., 2002. Structural evolution of the Andes in a transitional zone between flat and normal subduction (33.30°–33.45°S), Argentina and Chile, *J. South Am. Earth Sci.,* **15**(1), 101–116.

Giambiagi, L.B., Ramos, V.A., Godoy, E., Alvarez, P.P. & Orts, S., 2003. Cenozoic deformation and tectonic style of the Andes, between 33 and 34 south latitude, *Tectonics,* **22**(4), doi:10.1029/2001TC001354.

Gibert, G., Gerbault, M., Hassani, R. & Tric, E., 2012. Dependency of slab geometry on absolute velocities and conditions for cyclicity: insights from numerical modeling, *Geophys. J. Int.,* **189**(2), 747–760.

Gilbert, H., Beck, S. & Zandt, G., 2006. Lithospheric and upper mantle structure of central Chile and Argentina, *Geophys. J. Int.,* **165,** 383–398.

Gilbert, H., Velasco, A.A. & Zandt, G., 2007. Preservation of Proterozoic terrane boundaries within the Colorado Plateau and implications for its tectonic evolution, *Earth planet. Sci. Lett.,* **258**(1), 237–248.

Grevemeyer, I., Diaz-Naveas, J.L., Ranero, C.R. & Villinger, H.W., 2003. Heat flow over the descending Nazca plate in central Chile, 32 S to 41 S: observations from ODP Leg 202 and the occurrence of natural gas hydrates, *Earth planet. Sci. Lett.,* **213**(3), 285–298.

Grevemeyer, I., Kaul, N., Diaz-Naveas, J.L., Villinger, H.W., Ranero, C.R. & Reichert, C., 2005. Heat flow and bending-related faulting at subduction trenches: case studies offshore of Nicaragua and Central Chile, *Earth planet. Sci. Lett.,* **236**(1), 238–248.

Gutscher, M.A., Spakman, W., Bijwaard, H. & Engdahl, E.R., 2000. Geodynamics of flat subduction: seismicity and tomographic constraints from the Andean margin, *Tectonics,* **19**(5), 814–833.

Haberland, C., Rietbrock, A., Lange, D., Bataille, K. & Hofmann, S., 2006. Interaction between forearc and oceanic plate at the south-central Chilean margin as seen in local seismic data, *Geophys. Res. Lett.,* **33**(23), L23302, doi:10.1029/2006GL028189.

Hacker, B.R. & Abers, G.A., 2004. Subduction factory 3: an Excel worksheet and macro for calculating the densities, seismic wave speeds, and H_2O contents of minerals and rocks at pressure and temperature, *Geochem. Geophys. Geosyst.,* **5**(1), doi:10.1029/2003GC000614.

Hacker, B.R. & Abers, G.A., 2012. Subduction Factory 5: unusually low Poisson's ratios in subduction zones from elastic anisotropy of peridotite, *J. geophys. Res.,* **117**(B6), B06308, doi:10.1029/2012JB009187.

Hacker, B.R., Abers, G.A. & Peacock, S.M., 2003a. Subduction factory 1. Theoretical mineralogy, densities, seismic wave speeds, and H_2O contents, *J. geophys. Res.,* **108**(B1), doi:10.1029/2001JB001127.

Hacker, B.R., Peacock, S.M., Abers, G.A. & Holloway, S.D., 2003b. Subduction factory 2. Are intermediate-depth earthquakes in subducting slabs linked to metamorphic dehydration reactions? *J. geophys. Res.,* **108**(B1), doi:10.1029/2001JB001129.

Hamza, V. & Munoz, M., 1996. Heat flow map of South America, *Geothermics,* **25**(48), 599–656.

Haschke, M., Günther, A., Melnick, D., Echtler, H., Reutter, K.J., Scheuber, E. & Oncken, O., 2006. Central and southern Andean tectonic evolution inferred from arc magmatism, in *The Andes,* pp. 337–353, Springer.

James, D.E. & Snoke, J.A., 1994. Structure and tectonics in the region of flat subduction beneath central Peru: crust and uppermost mantle, *J. geophys. Res.,* **99**(B4), 6899–6912.

Jordan, T.E. & Allmendinger, R.W., 1986. The Sierra Pampeanas of Argentina: a modern analogue of Rocky Mountain foreland deformation, *Am. J. Sci.,* **286,** 737–764.

Kay, S.M. & Abbruzzi, J.M., 1996. Magmatic evidence for Neogene lithospheric evolution of the central Andean 'flat-slab' between 30°S and 32°S, *Tectonophysics,* **259**(1), 15–28.

Kay, S.M. & Gordillo, C.E., 1994. Pocho volcanic rocks and the melting of depleted continental lithosphere above a shallowly dipping subduction zone in the Central Andes, *Contrib. Mineral. Petrol.,* **117**(1), 25–44.

Kay, S.M. & Mpodozis, C., 2002. Magmatism as a probe to the Neogene shallowing of the Nazca plate beneath the modern Chilean flat-slab, *J. South Am. Earth Sci.,* **15,** 39–57.

Kay, S.M., Mpodozis, C., Ramos, V.A. & Munizaga, F., 1991. Magma source variations for mid–late Tertiary magmatic rocks associated with a shallowing subduction zone and a thickening crust in the central Andes (28 to 33°S), *Geol. Soc. Am. Spec. Papers,* **265,** 113–138.

Kendrick, E., Bevis, M., Smalley, R. Jr., Brooks, B., Vargas, R.B., Lauría, E. & Fortes, L.P.S., 2003. The Nazca–South America Euler vector and its rate of change, *J. South Am. Earth Sci.,* **16**(2), 125–131.

Kennett, B.L.N. & Engdahl, E.R., 1991. Traveltimes for global earthquake location and phase identification, *Geophys. J. Int.,* **105**(2), 429–465.

Kirby, S., Engdahl, R.E. & Denlinger, R., 1996. Intermediate-depth intraslab earthquakes and arc volcanism as physical expressions of crustal and uppermost mantle metamorphism in subducting slabs, in *Subduction Top to Bottom,* Geophysical Monograph Series, **96,** pp. 195–214, American Geophysical Union.

Kissling, E., Ellsworth, W.L., Eberhart-Phillips, D. & Kradolfer, U., 1994. Initial reference models in local earthquake tomography, *J. geophys. Res.,* **99**(B10), 19 635–19 646.

Klein, F.W., 2000. User's guide to HYPOINVERSE-2000 a Fortran program to solve for earthquake locations and magnitudes, *USGS Open File Report,* Draft 5/19.

Kley, J. & Monaldi, C.R., 1998. Tectonic shortening and crustal thickness in the Central Andes: how good is the correlation? *Geology,* **26**(8), 723–726.

Kopp, H., Flueh, E.R., Papenberg, C. & Klaeschen, D., 2004. Seismic investigations of the O'Higgins Seamount Group and Juan Fernández Ridge: aseismic ridge emplacement and lithosphere hydration, *Tectonics,* **23**(2), doi:10.1029/2003TC001590.

Latorre, D., Virieux, J., Monfret, T., Monteiller, V., Vanorio, T., Got, J.L. & Lyon-Caen, H., 2004. A new seismic tomography of Aigion area (Gulf of Corinth, Greece) from the 1991 data set, *Geophys. J. Int.,* **159**(3), 1013–1031.

Litherland, M. & Aspden, J.A., 1992. Terrane-boundary reactivation: a control on the evolution of the Northern Andes, *J. South Am. Earth Sci.,* **5**(1), 71–76.

MacDougall, J.G., Fischer, K.M. & Anderson, M.L., 2012. Seismic anisotropy above and below the subducting Nazca lithosphere in southern South America, *J. geophys. Res.,* **117**(B12), doi:10.1029/2012JB009538.

Manea, V.C., Pérez-Gussinyé, M. & Manea, M., 2012. Chilean flat slab subduction controlled by overriding plate thickness and trench rollback, *Geology,* **40**(1), 35–38.

Marot, M., Monfret, T., Pardo, M., Ranalli, G. & Nolet, G., 2013. A double seismic zone in the subducting Juan Fernandez Ridge of the Nazca Plate (32°S), central Chile, *J. geophys. Res.,* **118**(7), 3462–3475.

Martinod, J., Funiciello, F., Faccenna, C., Labanieh, S. & Regard, V., 2005. Dynamical effects of subducting ridges: insights from 3-D laboratory models, *Geophys. J. Int.,* **163**(3), 1137–1150.

Martinod, J., Husson, L., Roperch, P., Guillaume, B. & Espurt, N., 2010. Horizontal subduction zones, convergence velocity and the building of the Andes, *Earth planet. Sci. Lett.,* **299**(3), 299–309.

Martinod, J., Guillaume, B., Espurt, N., Faccenna, C., Funiciello, F. & Regard, V., 2013. Effect of aseismic ridge subduction on slab geometry and overriding plate deformation: insights from analogue modeling, *Tectonophysics,* **588,** 39–55.

Miranda, S., 2001. Gravity crustal model for an Andean section at 32°S considering upper mantle lateral density variation, *Rev. Bras. Geof.,* **18**(2), doi:10.1590/S0102-261×2000000200001.

Monteiller, V., Got, J.-L., Virieux, J. & Okubo, P.G., 2005. An efficient algorithm for double-difference tomography and location in heterogeneous media, with an application to Kilauea volcano, Hawaii, *J. geophys. Res.,* **110,** B12306, doi:10.1029/2004BJ003466.

Orozco, L.A., Favetto, A., Pomposiello, C., Rossello, E. & Booker, J., 2013. Crustal deformation of the Andean foreland at 31° 30′S (Argentina) constrained by magnetotelluric survey, *Tectonophysics,* **582,** 126–139.

O'Connell, R.J. & Budiansky, B., 1974. Seismic velocities in dry and saturated cracked solids, *J. geophys. Res.,* **79**(35), 5412–5426.

O'Driscoll, L.J., Richards, M.A. & Humphreys, E.D., 2012. Nazca-South America interactions and the late Eocene-late Oligocene flat-slab episode in the central Andes, *Tectonics,* **31**(2), doi:10.1029/2011TC003036.

Paige, C. & Saunders, M.A., 1982. LSQR: an algorithm for sparse linear equations and least squares problems, *ACM Trans. Math. Softw.,* **8,** 43–71.

Pardo, M., Comte, D. & Monfret, T., 2002. Seismotectonic and stress distribution in the central Chile subduction zone, *J. South Am. Earth Sci.,* **15**(1), 11–22.

Peacock, S.M., 2001. Are the lower planes of double seismic zones caused by serpentine dehydration in subducting oceanic mantle? *Geology,* **29**(4), 299–302.

Pesicek, J.D., Engdahl, E.R., Thurber, C.H., DeShon, H.R. & Lange, D., 2012. Mantle subducting slab structure in the region of the 2010 M8.8 Maule earthquake (30–40°S), Chile, *Geophys. J. Int.,* **191**(1), 317–324.

Podvin, P. & Lecompte, I., 1991. Finite difference computation of traveltimes in very contrasted velocity models: a massively parallel approach and its associated tools, *Geophys. J. Int.,* **105**(1), 271–284.

Poliakov, A. & Podladchikov, Y., 1992. Diapirism and topography, *Geophys. J. Int.,* **109**(3), 553–564.

Porter, R., Gilbert, H., Zandt, G., Beck, S., Warren, L., Calkins, J. & Anderson, M., 2012. Shear wave velocities in the Pampean flat slab region from Rayleigh wave tomography: implications for slab and upper mantle hydration, *J. geophys. Res.,* **117**(B11), doi:10.1029/2012JB009350.

Ramachandran, K. & Hyndman, R.D., 2012. The fate of fluids released from subducting slab in northern Cascadia, *J. geophys. Res.,* **3,** 121–129.

Ramos, V.A., Jordan, T.E., Allmendinger, R.W., Mpodozis, C., Kay, S.M., Cortés, J.M. & Palma, M., 1986. Paleozoic terranes of the central Argentine-Chilean Andes, *Tectonics,* **5**(6), 855–880.

Ramos, V.A., 2004. Cuyania, an exotic block to Gondwana: review of a historical success and the present problems, *Gondwana Res.,* **7**(4), 1009–1026.

Ramos, V.A., 2009. Anatomy and global context of the Andes: main geologic features and the Andean Orogenic cycle, in *Backbone of the Americas: Shallow Subduction, Plateau Uplift, and Ridge and Terrane Collision,* Geol. Soc. Am. Memoirs, No. 204, pp. 31–65, eds Kay, S.M., Ramos, V.A. & Dickinson, W.R., Geological Society of America.

Ramos, V.A., Cristallini, E.O. & Pérez, D.J., 2002. The Pampean flat-slab of the Central Andes, *J. South Am. Earth Sci.,* **15**(1), 59–78.

Ranalli, G., 1995. *Rheology of the Earth,* 2nd edn, Chapman and Hall, 413 pp.

Ranero, C.R., Villasenor, A., Morgan, J.P. & Weinrebe, W., 2005. Relationship between bend-faulting at trenches and intermediate-depth seismicity, *Geochem. Geophys. Geosyst.,* **6**(12), Q12002, doi:10.1029/2005GC000997.

Regnier, M., Chiu, J.M., Smalley, R. Jr., Isacks, B.L. & Araujo, M., 1994. Crustal thickness variation in the Andean foreland, Argentina, from converted waves, *Bull. seism. Soc. Am.,* **84,** 1097–1111.

Reynard, B., 2013. Serpentine in active subduction zones, *Lithos,* **178,** 171–185.

Sallarès, V. & Ranero, C.R., 2005. Structure and tectonics of the erosional convergent margin off Antofagasta, north Chile (23°–30°S), *J. geophys. Res.,* **110**(B6), doi:10.1029/2004JB003418.

Sanchez, G. *et al.*, 2013. The Argentinean National Network of Seismic and Strong-Motion Stations, *Seism. Res. Lett.,* **85**(5), 729–736.

Skinner, S.M. & Clayton, R.W., 2013. The lack of correlation between flat slabs and bathymetric impactors in South America, *Earth planet. Sci. Lett.,* **371,** 1–5.

Somoza, R. & Ghidella, M.E., 2005. Convergencia en el margen occidental de America del sur durante el Cenozoico: Subduccion de Nazca. Farallon y Aluk, *Rev. Asoc. geol. Argent.,* **60**(4), 797–809.

Springer, M., 1999. Interpretation of heat-flow density in the Central Andes, *Tectonophysics,* **306**(3), 377–395.

Takei, Y., 2002. Effect of pore geometry on *Vp*/*Vs*: from equilibrium geometry to crack, *J. geophys. Res.,* **107**(B2), ECV 6-1–ECV 6–12.

Tassara, A., 2005. Interaction between the Nazca and South American plates and formation of the Altiplano-Puna plateau: review of a flexural analysis along the Andean margin (15–34°S), *Tectonophysics,* **399**(1), 39–57.

Tassara, A., Götze, H.J., Schmidt, S. & Hackney, R., 2006. Three-dimensional density model of the Nazca plate and the Andean continental margin, *J. geophys. Res.,* **111**(B9), doi:10.1029/2005JB003976.

Toksöz, M.N., Johnston, D.H. & Timur, A., 1979. Attenuation of seismic waves in dry and saturated rocks: I. Laboratory measurements, *Geophysics,* **44**(4), 681–690.

Twiss, R.J. & Moore, E.M., 1992. Normal faults, in *Structural Geology,* Chap. 5, 1st edn, pp. 74–95, W. H. Freeman.

Unsworth, M. & Rondenay, S., 2013. Mapping the distribution of fluids in the crust and lithospheric mantle utilizing geophysical methods, in *Metasomatism and the Chemical Transformation of Rock,* pp. 535–598, Springer.

Van Hunen, J., Van den Berg, A.P. & Vlaar, N.J., 2001. Latent heat effects of the major mantle phase transitions on low-angle subduction, *Earth planet. Sci. Lett.,* **190**(3), 125–135.

Van Hunen, J., Van den Berg, A.P. & Vlaar, N.J., 2002. On the role of subducting oceanic plateaus in the development of shallow flat subduction, *Tectonophysics,* **352**(3), 317–333.

Van Hunen, J., Van den Berg, A.P. & Vlaar, N.J., 2004. Various mechanisms to induce present-day shallow flat subduction and implications for the younger Earth: a numerical parameter study, *Phys. Earth planet. Int.,* **146,** 179–194.

Wagner, L.S., Beck, S. & Zandt, G., 2005. Upper mantle structure in the south central Chilean subduction zone (30 to 36°S), *J. geophys. Res.,* **110**(B1), B01308, doi:10.1029/2004JB003238.

Wagner, L.S., Beck, S., Zandt, G. & Ducea, M.N., 2006. Depleted lithosphere, cold, trapped asthenosphere, and frozen melt puddles above the flat slab in central Chile and Argentina, *Earth planet. Sci. Lett.,* **245**(1), 289–301.

Wagner, L.S., Anderson, M., Jackson, J.M., Beck, S.L. & Zandt, G., 2008. Seismic evidence for orthopyroxene enrichment in the continental lithosphere, *Geology,* **36**(12), 935–938.

Ward, K.M., Porter, R.C., Zandt, G., Beck, S.L., Wagner, L.S., Minaya, E. & Tavera, H., 2013. Ambient noise tomography across the Central Andes, *Geophys. J. Int.,* **194**(3), 1559–1573.

Watanabe, T., 1993. Effects of water and melt on seismic velocities and their application to characterization of seismic reflectors, *Geophys. Res. Lett.,* **20**(24), 2933–2936.

Yáñez, G. & Cembrano, J., 2000. Tectonic models for ridge collision at a continental plate boundary: the case of Juan Fernández ridge and Chile rise, preliminary results, *Congr. geol. Chil.,* **9,** 649–654.

Yáñez, G., Cembrano, J., Pardo, M., Ranero, C. & Selles, D., 2002. The Challenger-Juan Fernández-Maipo major tectonic transition of the Nazca–Andean subduction system at 33–34° S: geodynamic evidence and implications, *J. South Am. Earth Sci.,* **15**(1), 23–38.